Medical University of Vienna

Institute of Pathophysiology and Allergy Research

(Head: Univ. Prof. Dipl.-Ing. Dr. Barbara Bohle)

Department of Cellular and Molecular Pathophysiology

Effects of advanced glycation end products (AGEs) on human epithelial cell lines

Bachelor thesis submitted for the fulfilment of the requirements for the degree of

BACHELOR OF SCIENCE (BSc)

University of Veterinary Medicine Vienna

submitted by

Wenninger Iris

External Supervisor: Sabine Geiselhart, PhD

Internal Supervisor: Tobias Käser, PhD

Vienna, July 2023

DECLARATION

Hereby, I declaire that this bachelor thesis, titled “Effects of advanced glycation end products (AGEs) on human epithelial cell lines”, submitted in partial fulfilment of the requirements for the Bachelor’s degree in Biomedicine and Biotechnology, is my original work, unless otherwise acknowledged and referenced.

Vienna, July 2023

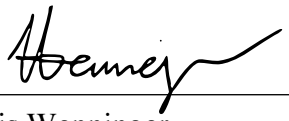

Iris Wenninger

ABSTRACT

Advanced glycation end products (AGEs) are a heterogeneous group of molecules formed by the non-enzymatic Maillard reaction. They either originate from exogenous sources (processed food, smoking) or are synthesized endogenously in the body. AGEs accumulate in human tissues during aging and are associated with various chronic diseases, such as diabetes mellitus and inflammatory bowel disease.

Human epithelia not only function as physical and biochemical barriers but have also been shown to be capable of initiating immune responses. Epithelial cells express many different pattern recognition receptors (PRRs), which initiate various downstream pathways when they are activated. RAGE, the receptor for AGEs, is also considered a PRR and was shown to play a role in mediating the effects of AGEs.

The aim of this work was to investigate the effects of AGEs on epithelial cells and to elucidate the role of RAGE in this context in an *in vitro* cell culture model.

Epithelial cells were analyzed for RAGE expression and localization by RT-qPCR and immunofluorescence microscopy (IFM), respectively. Intestinal epithelial cells were treated with glycated proteins as well as described ligands such as high mobility group box 1, S100 protein or anti-RAGE antibodies and analyzed for changes in signaling and gene expression.

RAGE is expressed in all cell lines tested, albeit at low levels compared to the lung. IFM revealed a vesicular pattern throughout the cell. Treatment of the cells resulted in activation of the ERK1/2 pathway, altered gene expression of tight junction proteins and cytokines, and changes in transepithelial resistance (TEER).

ZUSAMMENFASSUNG

Fortgeschrittene Glykierungs-Endprodukte (AGEs) gehören zu einer Gruppe heterogener Moleküle, die durch die nicht-enzymatische Maillard-Reaktion entstehen. Sie stammen entweder aus exogenen Quellen (verarbeitete Lebensmittel, Rauchen) oder werden im Körper endogen synthetisiert und reichern sich während des Alterns im menschlichen Gewebe an. Es wurde dabei erwiesen, dass AGEs bei vielen chronischen Krankheiten wie Diabetes mellitus und entzündlichen Darmerkrankungen eine Rolle spielen.

Das menschliche Epithel fungiert nicht nur als physikalische und biochemische Barriere, sondern ist auch in der Lage, Immunreaktionen auszulösen. Epithelzellen exprimieren viele verschiedene Pattern Recognition Rezeptoren (PRRs), die bei ihrer Aktivierung verschiedene nachgeschaltete Signalwege in Gang setzen. RAGE, der Rezeptor für AGEs, gilt ebenfalls als PRR und scheint an den Auswirkungen von AGEs beteiligt zu sein.

Ziel dieser Arbeit war es, die Auswirkungen von AGEs auf Epithelzellen zu untersuchen und die Rolle von RAGE in diesem Zusammenhang in einem *in vitro*-Zellkulturmodell zu erklären.

Epithelzellen wurden mittels RT-qPCR und Immunfluoreszenzmikroskopie (IFM) auf RAGE-Expression und -Lokalisierung untersucht. Intestinale Epithelzellen wurden mit glykierten Proteinen sowie beschriebenen Liganden wie High Mobility Group Box 1, S100-Protein oder Anti-RAGE-Antikörpern behandelt und auf Veränderungen der Signalübertragung und Genexpression untersucht.

RAGE wird in allen getesteten Zelllinien exprimiert, wenn auch in geringerem Maße als in der Lunge. IFM zeigte dabei ein vesikuläres Muster in der gesamten Zelle. Die Behandlung der Zellen führte zu einer Aktivierung des ERK 1/2-Signalwegs, einer veränderten Genexpression von Tight-Junction-Proteinen und Zytokinen sowie zu Veränderungen der transepithelialer elektrischen Resistenz (TEER).

ABBREVIATIONS

AB	Antibody
AGEs	Advanced glycation end products
AMPS	Amonium peroxodisulfate
BSA	Bovine Serum Albumin
C-domain	Constant domain
Caco-2 cells	Cancer coli-2 cells
Dia-1	Diaphanous-1
DPBS	Dulbecco´s Phosphate Buffered Saline
E-CAD	E-cadherin
EGF	Epidermal growth factor
esRAGE	Endogenously secreted receptor for advanced glycation end products
FBS	Fetal Bovine Serum
flRAGE	Full-length receptor for advanced glycation end products
HMGB1	High mobility group box 1
IBD	Inflammatory bowel diseases
IE	Intestinal epithelium
IECs	Intestinal epithelial cells
IL	Interleukin
JAM-A	Junctional Adhesion molecule A
LPA	Lysophosphatidic acid
MAMPs	Microbial-associated molecular patterns
MAPKs	Mitogen activated protein kinases
MCP-1	Monocyte Chemoattractant Protein-1
PAMPs	Pathogen-associated molecular patterns
PBS	Phosphate buffered saline
Pen-Strep	Penicillin-streptomycin
PRR	Pattern-recognition receptor
RAGE	Receptor for advanced glycation end products
ROS	Reactive oxygen species
SB	Sample buffer
SDS-PAGE	Sodium Dodecyl Sulfate – PolyAcrylamid Gel Electrophoresis

sRAGE	Soluble receptor for advanced glycation end products
TBS	Tris-buffered saline
TBST	Tris-buffered saline with Tween 20
TEER	Transepithelial electrical resistance
TEMED	Tetramethylethylendiamin
TNF-α	Tumor necrosis factor alpha
TSLP	Thymic stromal lymphopoietin
V-domain	Variable domain
ZBTB20	Zinc finger and BTB domain containing 20

TABLE OF CONTENTS

1. INTRODUCTION

1.1 Advanced glycation end products (AGEs)

1.1.1. Formation of AGEs

Advanced glycation end products (AGEs) are a heterogeneous group of molecules. They are formed through a non-enzymatic reaction called the Maillard reaction (Figure 1). During this process free carbonyl groups of reducing sugars such as glucose, fructose or ribose react with free amino groups of proteins, nucleic acids or lipids (Perrone, 2020). The reaction itself can be divided into several steps, starting with the condensation of a carbonyl group and an amino group which then produce a so-called Schiff base. This step is reversible and can further produce Amadori-products through Amadori-rearrangements, followed by the formation of reactive carbonyls such as methylglyoxal, glyceraldehyde or glyoxal, which then undergo irreversible transformation into AGEs through rearrangements (Twarda-Clapa et al., 2022).

Additionally, AGEs can arise through several pathways besides the Maillard reaction (Figure 1). These include the polyol pathway, glycolysis, glycose-oxidation and lipid-oxidation. The polyol pathway operates similarly to the Maillard reaction, with the distinction that, instead of an Amadori-product, a Heyns-product is formed through Heyns-rearrangement. Amadori- and Heyns-compounds are also summarized as early glycation products and must undergo further rearrangements to form the final AGEs (Twarda-Clapa et al., 2022).

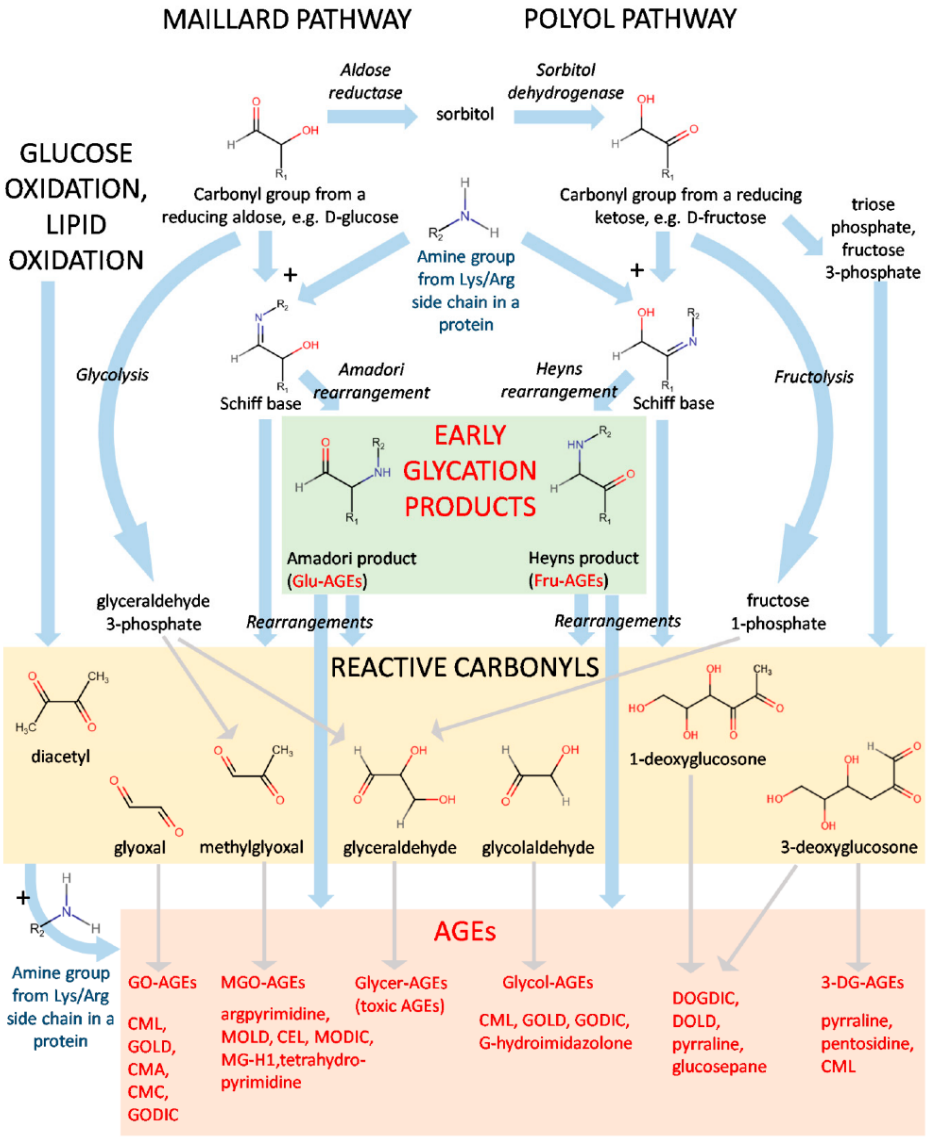

Figure 1. Formation of AGEs: Condensation of a carbonyl group and an amine group produce a Schiff base. Schiff bases are transformed into Amadori-products through Amadori-rearrangements which later form final AGEs (Twarda-Clapa et al., 2022).

1.1.2. Endogenous and exogenous origin

Advanced glycation endproducts can be formed endogenously (i. e., in the host), when long-lived proteins or other macromolecules encounter free circulating reducing sugars. Additionally, AGEs can arise from exogenous sources, including dietary intake and exposure to substances such as cigarette smoke. The Maillard reaction, catalyzed by heat during food processing methods such as baking, frying or cooking, leads to the formation of dietary AGEs.

As the consumption of thermally processed food and diets high in sugar has become more prevalent over time, the level of AGEs has correspondingly increased. This increase in AGEs correlates with the increased incidence of chronic diseases, which is a growing clinical and public health concern, particularly in Western countries (Cepas et al., 2020).

1.1.3. Pathophysiology

Advanced glycation endproducts have emerged as a key mediator in the development and progression of various chronic diseases (Gill et al., 2019). The AGEs formation on proteins and other macromolecules impairs their structure and eventually function. The accumulation of such molecules ultimately affects cell function and tissue homeostasis. Furthermore, the interaction between AGEs and the receptor for advanced glycation end products (RAGE), initiates a cascade of downstream signaling pathways. These pathways contribute to the development of pathologic conditions within the body (Cepas et al, 2020; Twarda-clapa et al., 2022), such as diabetes (Ramasamy et al., 2022), atherosclerosis (Singh et al., 2022), inflammatory bowel disease (IBD) (Boyapati et al., 2016), Alzheimer's disease (Chellappa et al., 2021), cancer (Muthyalaiah et al., 2021), and cardiovascular disease (Yubero-Serrano & Pérez-Martínez, 2020).

1.2. RAGE, receptor for advanced glycation end products

A range of receptors are involved in binding AGEs. These include the so-called scavenger receptors, which belong to the superfamily of membrane-associated proteins. Notable members of this receptor family encompass SR-A, CD36 and CD68 (Indyk et al., 2021).

Another important receptor is RAGE, which is a transmembrane receptor belonging to the immunoglobulin superfamily and family of cell adhesion molecules. It is highly expressed in the lung, but its expression is relatively low in other adult tissues under physiological conditions. However, in the presence of chronic inflammation or age-related diseases, RAGE expression seems to be upregulated (Bongarzone et al., 2017; Chiappalupi et al., 2021).

Through the process of alternative splicing, different variants of RAGE are formed. These are mainly full-length RAGE (flRAGE) and a C-truncated soluble form designated endogenous secretory RAGE (esRAGE) (Bongarzone et al., 2017).

RAGE can bind to various classes of ligands other than AGEs. These include calgranulins/S100 proteins, β-amyloid peptides, high mobility group box 1 (HMGB1), protein C1q and lysophosphatidic acid (LPA) (Dong et al., 2022).

All these ligands contribute to the initiation of multiple downstream processes that lead to changes in gene expression (Kim et al., 2021).

1.2.1. Structure of RAGE

Full-length RAGE can be divided into three regions: an extracellular domain, a transmembrane domain, and a cytoplasmic tail (Figure 2) (Bierhaus et al., 2005). The extracellular domain consists of one N-terminal variable domain (V-domain) and two constant domains (C1 and C2). It has been discovered that the V- and C1-domain also form a single integrated domain, known as VC1, which is connected to the C2-domain via a flexible linker. Notably, VC1 is considered to serve as the binding site for most RAGE ligands (Degani et al., 2017).

The cytoplasmic tail is important for intracellular signaling (Reed et al., 2020). Various binding adaptors may be critical for RAGE-mediated signal transduction, such as Diaphanous-1 (Dia-1), TIRAP and MyD88 (Sakaguchi et al., 2017). In addition, the oligomerization of RAGE, which is stabilized by intermolecular bridges in the C2-domain, is also important for signal transduction (Moysa et al., 2019).

Compared to flRAGE, esRAGE lacks the transmembrane and cytoplasmic domain; it is thus not bound to the cell membrane and can not induce intracellular signaling. Another soluble form is sRAGE, which is cleaved from flRAGE by matrix metalloproteinases and actively secreted by the cell (Dong et al., 2022).

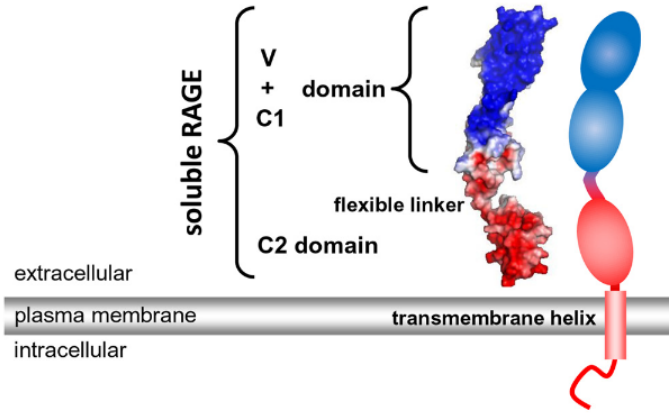

Figure 2. Structure of flRAGE and sRAGE: flRAGE consists of a VC1-, C2-domain, which are connected through a flexible linker, a transmembrane domain and a cytoplasmatic tail. sRAGE on the contrary does neither contain a transmembrane domain nor the cytoplasmic domain (Kierdorf & Fritz, 2013).

1.2.2. Signaling pathways

The interaction between RAGE and its ligands, including AGEs, initiates various downstream signaling pathways, such as the mitogen activated protein kinases (MAPKs) (ERK1/2, p38, SAPK/JNK), STAT3, Akt and GTPases (Racr1, Cdc42) signaling pathways (Hudson & Lippman, 2018).

Ultimately, most of these signaling pathways activate the transcription factor NF-κB. Under normal conditions, NF-κB is bound to its inhibitory protein IκB. However, the activation of RAGE signaling pathways result in the hydrolysis of IκB, leading to its dissociation from NF-κB. Consequently, NF-κB translocates to the nucleus, where it initiates the transcriptional expression of various inflammatory factors such as Interleukin-1 (IL-1), Tumor necrosis factor alpha (TNF- α) and Interleukin-6 (IL-6). The upregulation of these inflammatory factors can contribute to the development of chronic diseases, including diabetes and IBD (Yue et al., 2022).

NF-κB activation also triggers sustained RAGE-expression, creating a positive feedback loop that further amplifies the initial RAGE-mediated responses (Kierdorf & Fritz, 2013).

Finally, the binding of ligands to RAGE induces the activation of NADPH oxidase, leading to the formation of reactive oxygen species (ROS) (Taguchi & Fukami, 2023).

1.3. Epithelial barriers

The human epithelium plays a critical role as the primary interface regulating communication between the body and its external environment. Epithelia employ physical, chemical and immunological strategies to protect the body and are present in various body parts, including the skin, gastrointestinal tract and airways. By forming a continuous layer with minimal gaps between cells, the various epithelial tissues act as a protective wall. Nevertheless, there are variations in the structure and functionality of these barriers across different anatomical locations (Celebi Sözener et al., 2020).

1.3.1. Intestinal epithelium

Among these barriers, the intestinal epithelium (IE) is the largest, covering an expansive surface area of approximately 400 m^2. While a major function is the uptake of nutrients and water from ingested food, it also acts as a physical and biochemical barrier to the outer environment, protecting the body against harmful substances such as bacteria and toxins (Peterson & Artis, 2014).

The latter role has long been underestimated; it is now becoming increasingly clear that the IE is also an integral part of the immune system, instructing immune cells to initiate appropriate responses to external stimuli (Rescigno, 2011). Many pattern-recognition receptors (PRRs) are expressed by the IE, which recognize microbial signature molecules known as microbial/pathogen-associated molecular patterns (MAMPs/PAMPs). This recognition further initiates an immediate inflammatory response and is crucial for maintaining proper barrier function and immune homeostasis (Schoultz & Keita, 2020).

In addition to the PRRs, the IE is equipped with various transmembrane proteins, including tight junction and adherens junction proteins. These proteins contribute to tissue integrity and are essential for preserving intestinal homeostasis (Snelson et al., 2022). Various factors, such as growth factors, inflammatory signals like cytokines, and metabolites, create a complex microenvironment that regulates intestinal epithelial cells (IECs). Hence, an imbalance in the microenvironment of the IE can lead to gut barrier dysfunction, which is associated with several chronic diseases, such as IBD. Dysfunction not only affects the integrity of the IE but also

triggers inflammation and modulates the immune system. Therefore, maintaining the homeostasis of the gut barrier is important to prevent and manage these conditions effectively (Bonis et al., 2021; Creff et al., 2021; Snelson et al., 2022).

1.4. Caco-2 cells – an in vitro model to mimic the epithelial barrier

Cancer coli-2 (Caco-2) cells are epithelial cells which were first obtained from a human colon adenocarcinoma. Since then, they have been used as a model for the IE barrier as they show many morphological and functional characteristics of enterocytes of the small intestine (Kleiveland et al., n.d.; Sambuy et al., 2005). Furthermore, Caco-2 cells are immortalized and undergo self-differentiation upon reaching confluence. Notably, this spontaneous differentiation leads to the acquisition of their specialized features that closely resemble the IE (Figure 3). These include the development of microvilli, tight junctions, and a polarized structure with distinct apical, lateral, and basolateral domain. This polarization allows the formation of a semi-permeable and selective mucosal barrier that closely resembles the IE *in vivo* (Cao et al., 2012; Paul et al., 2023). Furthermore, they express intestinal enzymes such as sucrase-isomaltase, lactase or dipeptidylpeptidase IV (Sambuy et al., 2005).

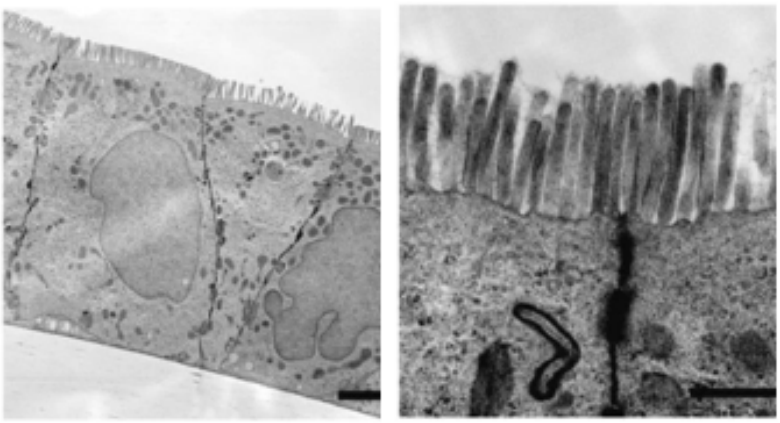

Figure 3. Differentiated Caco-2-cells: the cells exhibit characteristics of intestinal epithelial cells, including a polarized structure and the presence of microvilli, following their differentiation (Lopez-Escalera & Wellejus, 2022).

1.5. Aims of this thesis

The increase in immune-related diseases has been linked to our lifestyle habits, including dietary habits. AGEs have thus been recognized as influential factors in human health. However, it is not yet well understood how AGEs specifically affect epithelial cells.

The aim of this work was to investigate the effect of AGEs on epithelial cells, focusing mainly on IE. Thus, the majority of the experiments was performed with the *in vitro* intestinal model Caco-2 cells.

Scientific questions addressed in this thesis:

- What is the expression level of RAGE in Caco-2 cells and other selected epithelial cells in comparison to human lung tissue?
- What is the cellular localization of RAGE in Caco-2 cells and other selected epithelial cells?
- Do AGEs change the integrity of the cell monolayer in Caco-2 cells?
- Do AGEs induce changes in RAGE signaling pathways in Caco-2 cells?
- Does treatment with AGEs lead to changes in gene expression in Caco-2 cells ?

2. MATERIALS AND METHODS

2.1. Materials

2.1.1. Laboratory equipment and consumables

- 24-well cell culture plate (Thermo Fisher Scientific, USA)
- 25/75 cm^2 cell culture flask (TPP®, Switzerland)
- 6-well cell culture plate (VWR, Germany)
- 96-well-reaction-plate (Thermo Fisher Scientific, USA)
- Biorad Imager (ChemiDoc™ Imaging system, , Bio-Rad, Austria)
- Blotting apparatus (PerfectBlue Semi-dry electroblotter, VWR, Germany)
- Cell counter (Luna™ Automated Cell Counter, Logos Biosystems, Korea)
- Centrifuge (Centrifuge 5810 R, Eppendorf, Germany)
- Confocal Imager (UltraVIEW ERS Rapid ,Perkin-Elmer, USA)
- Confocal microscope (Axiovert 200M Inverted Microscope, Zeiss, Austria)
- Gel electrophoresis apparatus (Mini-PROTEAN® Tetra System, Bio-Rad, Austria)
- Image-iT Solution Fixative (Thermo Fisher Scientific, USA)
- Incubator (Cytoperm™ 2, Thermo Fisher Scientifics, USA)
- Laminar flow hood (Herasafe KS, Thermo Fisher Scientific, USA)
- Magnetic stirrer (C-MAG HS 10 digital, IKA, Germany)
- MicroAmp™ optical adhesive film (Thermo Fisher Scientific, USA)
- Microscope (CKX53 Cell Culture Microscope, OLYMPUS, Japan)
- Nitrocellulose membrane (Amersham™ Protran®, VWR, Germany)
- pH-Meter (913 pH Meter, Ω Metrohm, Swiss)
- Pipette tips (Biozym Scientific GmbH, Austria)
- Pipettes (Eppendorf, Germany)
- Precision scale (SQP-C, Sartorius, Germany)
- Reaction tubes 1.5 ml (Biozym Scientific GmbH, Austria)

- Shaker device (Rocker 2D digital, IKA, Germany)
- Spectrophotometer/Fluorometer (DS-11 FX+, DeNovix, USA)
- SuperSignal™ West Pico PLUS Chemiluminescent Substrate (Thermo Fisher Scientifics, USA)
- Thermocylcer (QuantStudio 5 Real-Time PCR System, Thermo Fisher Scientific, USA)
- Thermomixer (Thermomixer comfort, Eppendorf, Germany)
- Transwell inserts 6.5 mm, 24-well plate (Corning, USA)
- Voltohmmeter (EVOM2^{TM} Epithelial Voltohmmeter, WPI, USA)
- Vortex shaker (Vortex 3, IKA, Germany)
- Water bath (WNB 22, Memmert, Germany)
- µ-Slide 8 well (Ibidi, Germany)

2.1.2. Cells

- Human bronchial epithelial cell line – 16HBE14o- (Millipore, Cat. # SCC150) – kindly provided by Sabine Flicker, Inst. of Pathophysiology and Allergy Research; mRNA from these cells and cells cultured in chamber slides were provided by Sabine Geiselhart
- Intestinal epithelial cell line – Caco-2 (ATCC, HTB-37)
- Jurkat E6.1 cells (T cell line) overexpressing human flRAGE (UniProt Q15109) (generated by Peter Steinberger, Inst. of Immunology, Med. Univ. Vienna)
- mRNA from FHs 74 Int cells (a cell line with epithelial morphology, derived from healthy fetal small intestine) was provided by Sabine Geiselhart, Inst. of Pathophysiology and Allergy Research
- Total RNA from healthy human lung (Thermo Fisher Scientific, QS0618)

2.1.3. Chemicals and kits

- Acetic acid glacial 100 % (VWR, Germany)
- Acrylamid/Bis 40 % Solution 19:1 (Bio-Rad, Austria)
- Acrylamid/Bis 40 % Solution 37.5:1 (Bio-Rad, Austria)

- AGE-modified BSA was provided by Sabine Geiselhart, Inst. of Pathophysiology and Allergy Research
- Amonium peroxodisulfate (AMPS) ≥ 98 % (Sigma-Aldrich, Germany)
- Bromphenol blue (Sigma-Aldrich, Germany)
- DMEM (1x) + GlutaMAX™ (Thermo Fisher Scientifics, USA)
- Dulbecco´s Phosphate Buffered Saline (DPBS) (1x) (Thermo Fisher Scientifics, USA)
- DRAQ5™ (5 mM) (Thermo Fisher Scientifics, USA)
- Ethanol 96 % (Merck, Germany)
- Fetal Bovine Serum (Thermo Fisher Scientifics, USA)
- First Strand cDNA Synthesis Kit (Thermo Fisher Scientifics, USA)
- Glycerol 87 % (Merck, Germany)
- Glycine ≥ 99 % (Sigma-Aldrich, Germany)
- Halt™ Protease Inhibitor Cocktail 100x (Thermo Fisher Scientifics, USA)
- Hydrochlorid acid 37 % (VWR, Germany)
- Methanol ≥ 99.9% (Fisher Scientifics, Austria)
- N,N,N',N'-Tetramethylethylendiamin (TEMED) 99 % (Sigma-Aldrich, Germany)
- PageRuler™ Plus Prestained Protein Ladder (Thermo Fisher Scientifics, USA)
- Penicillin-Streptomycin (Pen-Strep) (100x) (Thermo Fisher Scientifics, USA)
- Phosphatase Inhibitor (Booster Immunoleader, USA)
- Ponceau S (Sigma-Aldrich, Germany)
- qPCR Human Reference Total RNA #63669 (Takara Bio, USA)
- Recombinant High mobility group box 1 (HMGB1) #1690-HMB (R&D Systems, USA)
- Recombinant Human epidermal growth factor #585506 (Biolegend, USA)
- Recombinant Human S100A12 (EN-RAGE CF) #1052-ER (R&D Systems, USA)
- RNeasy® Mini Kit (QIAGEN, Germany)
- RNase-free water (Sigma-Aldrich, Germany)
- RPMI Medium 1640 (1x) + GlutaMAX™ (Thermo Fisher Scientifics, USA)
- Saponin (Sigma-Aldrich, Germany)
- Serum from donkey, serum from goat (Sigma-Aldrich, Germany)
- Skim milk powder (Sigma-Aldrich, Germany)

- Sodium chloride (Sigma-Aldrich, Germany)
- Sodium dodecyl sulfate ≥ 98.5 % (Sigma-Aldrich, Germany)
- SYBR™ Green PCR Master Mix (Thermo Fisher Scientifics, USA)
- Tumor necrosis factor alpha (TNF-α) #300-01A (Peprotech, USA)
- Tris(hydroxylmethyl)amino-methane ≥ 99.9 % (Sigma-Aldrich, Germany)
- Triton X-100 (Thermo Fisher Scientifics, USA)
- Trypsin-EDTA 0.25 % (1x) (Thermo Fisher Scientifics, USA)
- β-Mercaptoethanol ≥ 99.9% (Merck, Germany)

2.1.4. Antibodies (AB) used for Western blotting and immunofluorescence microscopy

Table 1. Primary and secondary antibodies

Antibody	Type, source	Dilution	Company, Cat no.
RAGE	Monoclonal mouse IgG2B Clone 176902		R&D Systems (USA), MAB11451
Isotype	Monoclonal mouse IgG2B Clone 20116		R&D Systems (USA), MAB004
RAGE (A11)	Monoclonal mouse IgG2A/κ	1:50	Santa Cruz Biotechnology (USA), sc-80652
RAGE	Polyclonal Goat IgG	1:50/ 1:100	R&D Systems (USA), AF1145
Phospho-p38α	Monoclonal, mouse IgG2A, Clone #696602	1:250	R&D Systems (USA), MAB8691
Phospho-p44/42 MAPK (Erk1/2)	Monoclonal, rabbit IgG Clone D13.14.4E	1:500	Cell Signaling Technology (USA), 4370
IκBα	Polyclonal, rabbit IgG	1:500	Cell Signaling Technology (USA), 9242
Tubulin	Polyclonal, rabbit IgG	1:2 500	Cell Signaling Technology (USA), 2144
anti-rabbit IgG-HRP	goat	1:20 000	Abcam (UK), Ab97051
anti-mouse IgG-HRP	rabbit	1:20 000	Abcam (UK), Ab97046

Anti-goat IgG-AlexaFluor-488	donkey	1:2000	ThermoFisher Scientific (USA), A-11055
Anti-mouse IgG-AlexaFluor-488	goat	1:2000	ThermoFisher Scientific (USA), A-11001

2.1.5. Buffer and solutions

Activation of cells

Table 2. Lysis buffer

Reagents	Volume/Weigth
Tris (50 mM)	5.844 g
NaCl (150 mM)	12.114 g
Titron X-100 (1 % v/v)	1 ml
Aqua bidest (A. bidest)	to final volume of 100 ml
HCl (5 M)	Adjust to pH 8

Table 3. Lysis buffer with protein and phosphatase inhibitors

Reagents	Volume
Lysis buffer	1 ml
EDTA (100x)	10 µl
Phosphatase inhibitor (100x)	10 µl
Protease inhibitor (100x)	10 µl

Sodium Dodecyl Sulfate – PolyAcrylamid Gel Electrophoresis (SDS-PAGE)

Table 4. 3 M Tris-HCl, pH 8.8

Reagents	Volume/Weigth
Tris (50 mM)	181.7g
Aqua bidest (A. bidest)	to final volume of 500 ml
HCl (5 M)	Adjust to pH 8.8

Table 5. 0.5 M Tris-HCl, pH 6.8

Reagents	Volume/Weigth
Tris (50 mM)	6.1g
Aqua bidest (A. bidest)	to final volume of 100 ml
HCl (5 M)	Adjust to pH 6.8

Table 6. Reducing SDS-PAGE sample buffer (4x stock solution)

Reagents	Volume/Weigth
Tris-HCl (250 mM)	5 ml
Glycerol (30 % v/v)	3 ml
SDS (8 % w/v)	0.8 g
β-Mercaptoethanol (20% v/v)	2 ml
Bromphenol blue (0.05 % w/v)	5 mg

Table 7. Running buffer (10x stock solution)

Reagents	Volume/Weigth
Tris (0.25 M)	30 g
Glycine (1.92 M)	144 g
SDS (1 % w/v)	10
A. bidest	to final volume of 1000 ml

Western blot

Table 8. Transfer buffer

Reagents	Volume/Weigth
Tris (48 mM)	5.8 g
Glycine (39 mM)	2.93 g
SDS (0.0375 % w/v)	0.375 g
Methanol (20 % v/v)	200 ml
A. bidest	to final volume of 1000 ml

Table 9. Ponceau red staining buffer

Reagents	Volume/Weigth
Ponceau red (0.1 % w/v)	0.5 g
Acetic acid (5 % v/v)	25 ml
A. bidest	to final volume of 500 ml

Table 10. Ponceau red distaining buffer

Reagents	Volume
Acetic acid (1 % v/v)	5 ml
A. bidest	to final volume of 500 ml

Table 11. 10x Tris-buffered saline (TBS)

Reagents	Volume/Weigth
Tris	61 g
NaCl	88 g
A. bidest	to final volume of 1000 ml
HCl (5 M)	Adjust to pH 7.4

Table 12. Wash buffer (1x Tris-buffered saline with Tween20 (TBST))

Reagents	Volume
10x TBS	200 ml
Tween (0.1 % v/v)	2 ml
A. bidest	to final volume of 2000 ml

Table 13. Blocking buffer

Reagents	Volume/Weigth
Milk powder (5 % w/v)	2.5 g
1x TBST	50 ml

2.2. Methods

2.2.1. Cultivation of cells

Caco-2 cells were cultivated in DMEM GlutaMAX medium and Jurkat cells in RPMI GlutaMAX. Media were supplemented with 10 % Fetal Bovine Serum (FBS) and 1 % penicillin-streptomycin (Pen-Strep). The cells were maintained in a humidified incubator at 37 °C with 5 % CO_2. When cells reached 80-90 % confluence, they were passaged. For passaging Caco-2 cells (adherent cells), the medium was removed from the flask and cells were washed with PBS. To detach the cells from the flask, 0.25 % Trypsin-EDTA was used. Detached cells were then transferred into a reaction tube, followed by centrifugation at 300 x *g* for 5 minutes. Cells were resuspended in 1 ml of medium and split 1:4. Jurkat cells (suspension cells) were split every other day. Cells were first resuspended with the medium in the flask, then ¾ of the old medium was replaced with fresh medium.

2.2.2. Transepithelial electrical resistance (TEER)

Caco-2 cells were counted using the LUNATM Automated Cell Counter (Logos Biosystem) following the manufacturer's instructions. Plates with transwell inserts (0.4 µm polyester membrane) were prepared by adding 700 µl of medium to the basolateral chamber (the well below the insert) and 150 µl of Caco-2 cell suspension at a seeding density of 50,000 cells into the apical chamber (the transwell insert).

To monitor the integrity of the Caco-2 cell monolayers in the transwell inserts, TEER measurements were performed using the EVOM2^{TM} (Epithelial Voltohmmeter). Prior to measurements, transwell plates were brought to room temperature. The endohmmeter chamber of the EVOM2 system was sterilized with 70 % ethanol for 20 minutes, the ethanol was discarded, and 1.2 ml of medium were added to the chamber. The electrodes of the EVOM2 system were connected to the meter and the chamber, and the function of the meter was set to Ohm to measure the resistance values. The transwell inserts, starting with the blank resistance control (transwell insert without cells), were sequentially transferred into the chamber, and measurements were performed. Finally, the cells were returned to the incubator, and the Endohm chamber was cleaned. To calculate TEER, the surface area of the transwell (in cm^2) is multiplied by the NET resistance, which is the resistance measured minus the resistance of a blank transwell covered by cell culture media. Values are given as ohm*cm^2.

2.2.3. Activation of Caco-2 cells and preparation of cell lysates

Caco-2-cells were seeded in 24-well plates at a density of 30.000 – 50.000 cells per well in 1 ml of medium. The cells were cultured at 37 °C for approximately seven days until they reached confluence.

Prior to activation, the test substances EGF (epidermal growth factor), a RAGE-specific antibody (α-RAGE, MAB11451; Table 1), an isotype control (Table 1), S100A12, HMGB1 and AGE modified BSA (Bovine Serum Albumin; AGE-BSA) were prepared at the respective concentrations indicated in the result section. They were either diluted in phosphate buffered saline (PBS), if an excess amount of test substances was prepared and stored afterwards at -20 °C, or in cell culture medium, if only the required amount was prepared. The lysis buffer was

prepared (Table 2 + 3) and placed on ice together with PBS for precooling. The test substances were added to the cells and the plates were incubated at 37 °C for the time intervals indicated in the result section. Addition of the test substances was done in reverse order so that all samples could be harvested at the same time.

Finally, the plates were placed on ice, and the medium was removed. Cells were washed twice with PBS, then 50 µl of lysis buffer were added to each well. After 5 minutes of incubation, cells were harvested by pipetting up and down while also gently scratching the bottom of the well with the pipette tip. The samples were then transferred to precooled reaction tubes and immediately frozen and stored at -20 °C for further analyses of RAGE downstream pathways (p38, NF-κB and ERK 1/2).

2.2.4. SDS-PAGE

First, the gel apparatus was assembled following the manufacturer's instructions (Biorad). The separating gel (Table 14) was prepared, using Tris-HCl pH 8.8 (Table 4), and then poured in the apparatus. To ensure a smooth gel surface, a layer of isopropanol was carefully applied on top of the gel. After 30 minutes, the gel polymerized, and the excess isopropanol was poured off. Subsequently, the stacking gel (Table 14) was prepared, using Tris-HCl pH 6.8 (Table 5), added on top of the separating gel and the comb was positioned to generate loading wells. After one hour, during which the gel fully polymerized, it was ready for loading.

Table 14. Recipe for gels

Reagents	Stacking gel (4 %)	Separation gel (10 %/12 %)
Acrylamide (40 %) 19:1	150 µl	-
Acryamide (40 %) 37.5:1	-	1.6 ml/1.9 ml
Tris-HCl	190 µl	600 µl
SDS (10 %)	15 µl	50 µl
A. bidest	1.16 ml	3.5 ml/3.2 ml
AMPS (10 %)	15 µl	50 µl
TEMED	2 µl	5 µl

The gel was transferred into a casting frame and filled with 1x running buffer, which was prepared by mixing 1 volume of 10x stock solution (Table 7) and 9 volumes of A. bidest. The comb was removed by pulling it up straight, creating slots in the gel. Prior to loading, samples were prepared by adding 4x reducing SDS-PAGE sample buffer (SB; Table 6) until a concentration of 1x SB was achieved. Samples were then carefully pipetted into the slots. A molecular weight marker (PageRuler^{TM} Plus Prestained Protein Ladder) was included and all empty wells were filled with 1x SB. Finally, the electrophoresis was performed at a constant voltage of 120 V until the blue front (Bromphenol blue in the SB) had run out.

2.2.5. Western blot

Nitrocellulose membranes, cut the same size as the gel (80 mm x 70 mm), were utilized. The membrane and the gel from the SDS-PAGE, were then equilibrated and kept in transfer buffer (Table 8). Two filter papers the same size as the membrane were soaked in transfer buffer. The components were then stacked in the semidry blotter in the following order: anode (blotting surface) – filter paper – membrane – gel – filter paper – cathode (lid). Air bubbles were removed, and proteins were transferred at 15 V for 45 minutes.

After the transfer, the apparatus was disassembled, and the proteins on the membrane were stained with Ponceau red staining buffer (Table 9) for 5 minutes and distained in Ponceau red distaining buffer (Table 10) for 5 minutes to visualize the quality of the transfer.

The membranes were blocked in 10 ml of blocking buffer (Table 13) for one hour at room temperature or overnight at 4 °C. After blocking, the membranes were incubated with the respective primary antibodies for two to three hours at room temperature or overnight at 4 °C. Membranes were placed on a shaker during all incubation steps.

Antibodies were diluted in blocking buffer or 1 x TBST (Table 11 + 12), and dilutions are given in Table 1.

The membranes were then incubated with the respective primary antibody for three hours at room temperature or overnight at 4 °C.

After incubation, the membranes were washed three times with 1x TBST for a duration of 5 minutes. The secondary antibody solution was diluted according to Table 1, using either

blocking buffer or 1x TBST. The membrane was then incubated for two hours at room temperature.

The visualization of antibody binding was performed using chemiluminescence. The membranes were washed three times for 5 minutes in 1x TBST and then overlaid with the chemiluminescence mixture containing a 1:1 ratio of solution A and B (1 ml of each per membrane). After an incubation of 5 minutes, the membranes were placed in the Biorad Imager, allowing visualization of the bindings.

2.2.6. Indirect immunofluorescence microscopy

Adherent cells (Caco-2 and HBE cells) were cultured on chamber slides until they reached confluency and fixed with Image-iT™ Fixative Solution for 15 minutes. Suspensions cells (Jurkat cells) were treated according to a protocol by Tsang and colleagues (Tsang et al., 2017). Briefly, cells were pelleted by centrifugation, washed with PBS, and resuspended in PBS at a concentration of 1 x 10^6 cells/ml. Cells were transferred into the chamber slide and left at room temperature for 30 minutes to allow sedimentation. After careful removal of non-adherent cells, cells were fixed with Image-iT™ Fixative Solution for 15 minutes and washed twice with PBS for 5 minutes with gentle shaking. After blocking and permeabilization in 1x PBS containing 5 % (v/v) donkey or goat serum (corresponding to the host of the secondary antibody) and 0.05 % (w/v) saponin for 20 minutes, cells were incubated with the primary antibodies in blocking solution for two hours.

The slides were washed twice with PBS for 5 minutes, followed by incubation with the secondary antibody. The secondary antibodies were prepared in the same way as the primary antibodies and incubated for two hours at room temperature in the absence of light. The cells were again washed twice with PBS for 5 minutes.

For nuclear staining, DRAQ5 was diluted 1:1000 in PBS and added to the cells for a 10-minute incubation at room temperature, also protected from light.

Finally, cells were washed twice with PBS and covered with 350 µl of PBS per well. The slides were then analyzed by confocal microscopy. Images were acquired using an UltraVIEW ERS Rapid Confocal Imager (Perkin-Elmer) connected to a Zeiss Axiovert 200 microscope. Pictures

were processed by Volocity software (Version 5.5, Perkin Elmer). Files were exported and further processed with Image J (Version 1.54d) using identical conditions for positive stainings and negative controls. If needed, slides could be stored at 4 °C protected from light.

2.2.7. RNA isolation

Total RNA was extracted from treated as well as untreated cells using the RNeasy kit (Qiagen) following the manufacturer's instructions. Buffers, spin columns and collection tubes were included in the RNeasy kit. Briefly, cells were harvested with 350 µl RTL buffer containing 10 µl β-mercaptoethanol per 1 ml of buffer. An equal volume of 70 % ethanol was added to the homogenized lysate and mixed by pipetting. The mixture was then transferred to a RNeasy spin column placed in a 2 ml collection tube and centrifuged at 8000 x *g* for 15 seconds. The flow-through was discarded and 700 µl of RW1 buffer were added to the spin column and centrifuged for 15 seconds at 8000 x *g* followed by two washing steps with 500 µl of RPE buffer. The spin column was dried by an additional centrifugation step of 2 minutes at 8000 x *g* and placed in a new 1.5 ml collection tube. Then, 35 µl of RNase-free water was directly added to the spin column. RNA was then eluted by centrifuging for 1 minute at 8000 x *g* and RNA concentrations were measured using the Spectrophotometer/Fluorometer DeNovix DS-11 FX+. Samples were directly used for cDNA synthesis or stored at -20 °C for downstream RT-qPCR analysis.

2.2.8. Two-Step RT-qPCR

<u>cDNA synthesis</u>:

Total RNAs were converted into cDNAs using the First Strand cDNA synthesis kit. Briefly, 0.5 µg of RNA were mixed with 1 µl oligo dT and nuclease-free water was added to a volume of 10 µl. The mixture was incubated at 70 °C for 5 minutes, followed by immediate cooling on ice. The reaction mix (Table 15) was prepared and added to each sample. The samples were then incubated at 37 °C for one hour and stored at -20 °C until further use.

Table 15. cDNA synthesis reaction mix

Reagents	Volume (10µl/reaction)
5x Reaction buffer	4 µl
dNTPs	2 µl
Reverse transcriptase	2 µl
RNase inhibitor	1 µl
Nuclease-free water	1 µl

PCR analysis**:**

For the subsequent PCR step, the cDNA was diluted 1:10 with RNase-free water and placed on ice. The master mix (Table 16) was prepared and dispensed into the wells of an PCR-plate. Primers sequences are displayed in Table 17. One µl of DNA template was added to the wells. Each template was analyzed in triplicates and additionally triplicate negative controls were prepared in absence of any DNA template. The plate was carefully sealed, spined down and placed into the Thermocycler (Thermo Fisher Scientific).

The RT-qPCR was then initiated with the following programm:

1. HOLD Stage (1 cycle): 50 °C for 2 minutes, 95 °C for for 10 minutes
2. PCR Stage (40 cylces): 95 °C for 15 seconds, 60 °C for 1 minute
3. Melt Curve Stage (1 cylce): 95 °C for 15 seconds, 60 °C for 1 minute, 95 °C for 15 seconds

Table 16. Master mix preparation protocol

Reagents	Volume (11µl/reaction)
SYBR Green PCR Master Mix	6 µl
Forward primer (5 pmol)	0.5 µl
Reverse primer (5 pmol)	0.5 µl
Nuclease free water	4 µl

Table 17. Primer sequences

Gene	Foward primer	Reverse primer
RAGE	GCTTGGAAGGTCCTGTCTCC	CACGGACTCGGTAGTTGGAC
JAMA	TTTACAGCCAGCCTAGTGCC	CGGTAGCACCTGAGTAAGGC
Claudin 1	CTGGGAGGTGCCCTACTTTG	ACACGTAGTCTTTCCCGCTG
Claudin 5	AAGTGTACGACTCGGTGCTG	AAACAGGTAGAGCACGCCTC
E-CAD	AGTGACTGATGCTGATGCCC	AATGTACTGCTGCTTGGCCT
IL-6	ACTCACCTCTTCAGAACGAATTG	CCATCTTTGGAAGGTTCAGGTTG
MCP-1	AGAGGCTGAGACTAACCCAGA	TTTCATGCTGGAGGCGAGAG
TSLP	GCCTTAGCTATCTGGTGCCC	GAAGCGACGCCACAATCCT
HMGB1	AGCCGAGAGGCAAAATGTCA	AGCAGACATGGTCTTCCACC
ZBTB20	CTGGCACTCACATACCCACA	TTGGCCTCGGCTAAGAGATG
GAPDH	GTCTCCTCTGACTTCAACAGCG	ACCACCCTGTTGCTGTAGCCAA
RPLP0	AATCTCCAGGGGCACCATTG	CAGGGTTGTAGATGCTGCCA

Calculation of relative gene expression:

For analyzing the relative changes in gene expression the $2^{-\Delta\Delta CT}$ method was used. First, the ΔCT value, which is the difference in the Ct value of the gene of interest and reference gene (GAPDH, RPLP0; Table 17) was calculated for all RT-qPCR samples. The obtained ΔCT value of each treated sample was then subtracted from the ΔCT value of the control sample, which is then known as ΔΔCT. The ΔΔCT value was then converted into a fold change value using the formula $2^{-\Delta\Delta CT}$.

3. RESULTS

3.1. RAGE mRNA expression in Caco-2 cells

First, we compared RAGE expression levels in Caco-2 (colon-derived IEC) with the expression levels in lung tissue and a lung-derived cell line (HBE), using RT-qPCR, as summarized in 2.2.8. We also included FHs 74 Int cells (healthy fetal small intestine-derived IEC) in this assay.

As expected, lung tissue exhibited by far the highest level of RAGE expression. Human lung-derived HBE cells also showed high RAGE expression compared to the both IECs. FHs 74 Int showed the lowest expression level (Figure 4).

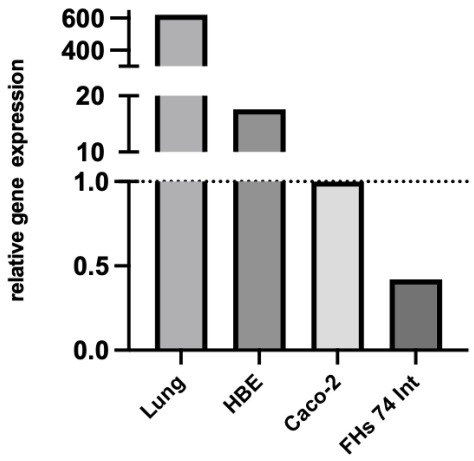

Figure 4. Relative gene expression of RAGE within different cell lines: Gene expression was analyzed with RT-qPCR. Results are given relative to Caco-2 cells and are shown as fold-change in gene expression

3.2. RAGE localization in Caco-2 cells

Immunofluorescence stainings were performed, as summarized in 2.2.6, to determine the localization of RAGE in Caco-2 cells. JE6-1 cells overexpressing flRAGE were used as a positive control, the lung-derived epithelial cell line HBE was also included.

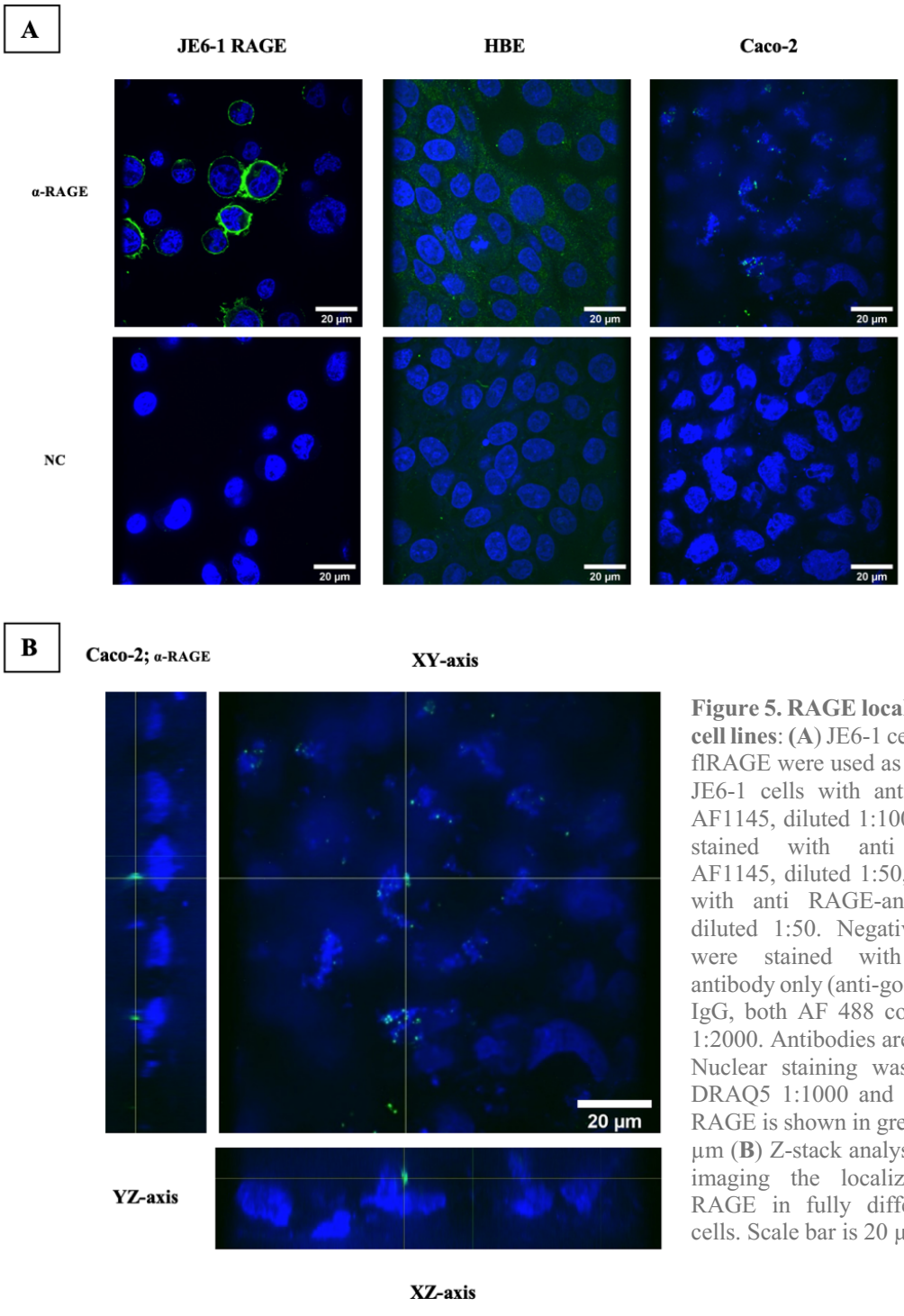

Figure 5. RAGE localization in human cell lines: **(A)** JE6-1 cells overexpressing flRAGE were used as a positive control. JE6-1 cells with anti RAGE-antibody AF1145, diluted 1:100; HBE-cells were stained with anti RAGE-antibody AF1145, diluted 1:50, and Caco-2 cells with anti RAGE-antibody SC A11, diluted 1:50. Negative controls (NC) were stained with the secondary antibody only (anti-goat IgG; anti-mouse IgG, both AF 488 conjugated), diluted 1:2000. Antibodies are given in Table 1. Nuclear staining was performed with DRAQ5 1:1000 and is shown in blue; RAGE is shown in green. Scale bar is 20 µm (**B**) Z-stack analysis of Caco-2 cells imaging the localization pattern of RAGE in fully differentiated Caco-2 cells. Scale bar is 20 µm.

All cells were stained with RAGE-specific antibodies (SC A11 and AF1145) and Figure 5 shows representative images.

As shown in Figure 5A, JE6-1 RAGE cells express RAGE on the cell surface. In human lung-derived HBE cells, RAGE was observed within versicular structures distributed throughout the cytoplasm. No such signals were observed in control stainings lacking the primary antibody.

In the intestine-derived Caco-2 cell line, RAGE was found to be localized in more distinct areas, showing a punctuate pattern (Figure 5A). Given that Caco-2 cells display a polarized structure, further investigations using ImageJ (Version 1.54d) were conducted to determine whether RAGE localization was apical or basolateral. By viewing the XZ-axis and YZ-axis (Figure 5B), it became visible that RAGE is localized at the apical aspect of the cells.

3.3. Modeling the intestinal epithelium

In all subsequent experiments, Caco-2 cells were used to evaluate the effects of AGEs on the intestinal epithelium, as these cells have higher RAGE expression compared with FHs 74 Int cells and are known to fully differentiate into a monolayer upon confluence. Caco-2 cells were grown on transwell inserts (semipermeable membranes) to improve morphological differentiation and to have the possibility of treating the cells from both the apical and basolateral side.

First, the TEER of the cells was studied, following the steps mentioned in 2.2.2, as this is a widely accepted quantitative method to measure the integrity of tight junction dynamics in cell culture models. Cells were seeded in transwell inserts and grown for 3 weeks. To follow the differentiation and evaluate the integrity of the cell monolayer of Caco-2 cells, regular TEER-measurements were conducted.

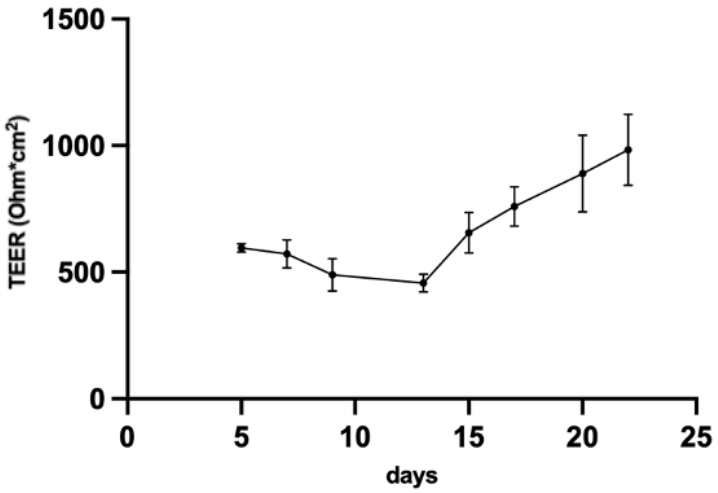

Figure 6. Assessment of cell monolayer integrity of Caco-2 cells: Cells were grown in transwell inserts. Integrity was assessed by measuring the transepithelial resistance (TEER), shown as dots. Measurements were performed over 3 weeks. Error bars ± represent standard deviations of individual monolayers.

TEER measurements were conducted with a total of 30 transwell inserts, and the results are presented in Figure 6. Due to possible disruption of the monolayer while exchanging the medium during the cultivation process, outliers were removed from the results prior to analysis, to get more reliable outcomes. As shown in Figure 6, TEER values started at 600 Ohm*cm^2 on

day 5, followed by a slight decrease until day 12. Subsequently, TEER values continuously increased and reached a relatively stable value of ≥ 800 Ohm*cm^2 after three weeks of differentiation. These results indicated an increase in monolayer integrity over a span of 22 days.

3.3.1. Changes in monolayer integrity after treatment with AGEs

After full differentiation, monolayers were treated with the different RAGE ligands from the apical as well as the basolateral side for one and four hours, as summarized in 2.2.3, and the integrity of the monolayers was examined after treatment. Non-treated cells (NC) were used as a control. A RAGE-specific antibody (α-RAGE) known to activate RAGE in a reporter cell system (unpublished data) was used as a positive control. The respective isotype served as a control to test for unspecific effects. Further, S100A12 and HMGB1, two well-described RAGE ligands, as well as chemically modified BSA (AGE-BSA) were used for activation (Figure 7). Notably, the experiment was only performed once.

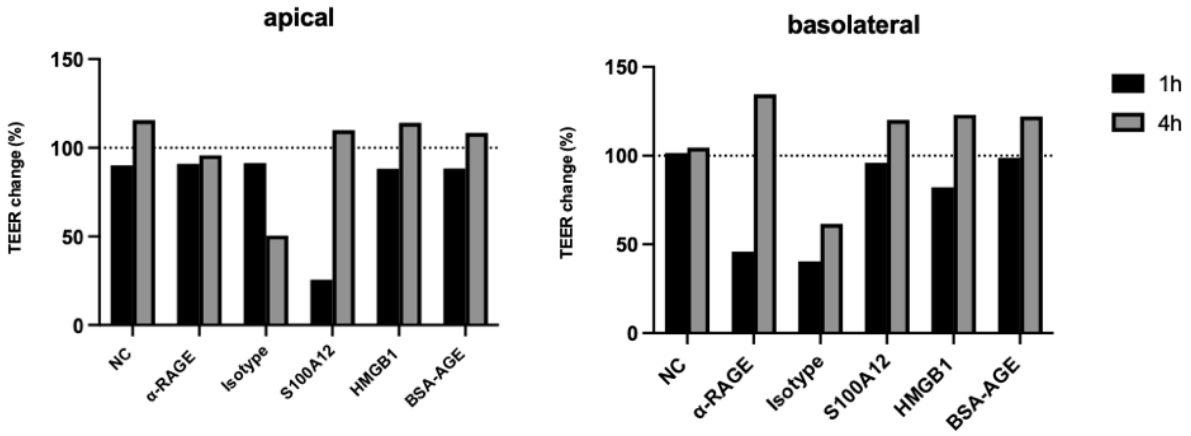

Figure 7. Effects of RAGE ligands on cell monolayer integrity of Caco-2 cells: Cells were either treated basolateral or apical with α-RAGE, an isotype control, S100A12 HMGB1 and BSA-AGE for one or four hours. NC represents untreated cells. TEER-measurements were performed before adding the ligands (pre-activation) and after incubation times (post-activation). Pre-and post- activation TEER values was compared and obtained results are given in % (y-axis). Dashed line represents pre-activation value (100%).

As shown in Figure 7, apical addition of α-RAGE, HMGB1 and BSA-AGE did not lead to changes in TEER compared to the negative control. Interestingly, addition of the isotype control led to a decrease after four hours of treatment with a reduction of 50 %. Treatment with

S100A12 even caused a reduction in TEER of 75 % after one hour, albeit addition for four hours showed no such change.

Basolateral addition of S100A12, HMGB1 and BSA-AGE caused a 20 to 23 % increase in TEER after four hours and variable effects after one hour. Treatment with α-RAGE resulted in a 54 % reduction of TEER after one hour. Controversy, the addition of α-RAGE for four hours showed a pronounced increase in TEER by 35 %. Interestingly, the isotype control resulted in a decrease in TEER after both one and four hours with a reduction of 60 and 38 % of TEER, respectively.

To summarize, AGE-BSA treatment of IECs had no major impact on the integrity of the monolayer.

3.4. Effect of RAGE-ligands on signaling pathways

To elucidate the effects of treatment of monolayers with RAGE-ligands on different downstream signaling pathways, immunoblotting (Western blot), according to 2.2.5, was performed, and results were quantified compared to a negative control (NC; non-treated cells). Briefly, activation of the pathways p38 (phosphorylation of p38), NF-κB (IκB degradation) and ERK1/2 (phosphorylation of p44/42) was assessed after stimulation with RAGE-ligands, including epidermal growth factor (EGF) as a positive control, a RAGE-specific antibody (α-RAGE) and HMGB1, in Caco-2-cells (Figure 8).

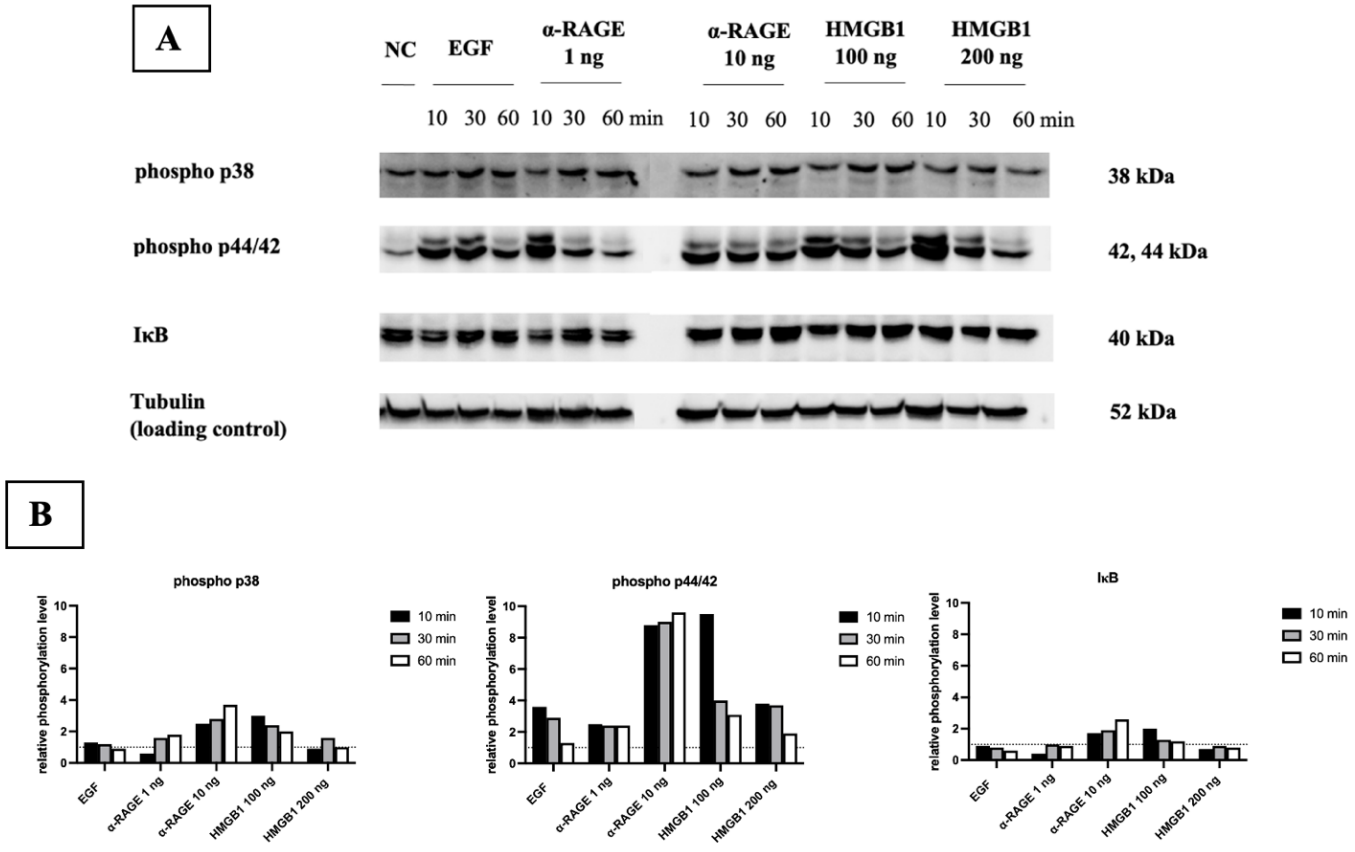

Figure 8. Activation of signalling pathways in Caco-2 cells after treatment with RAGE ligands: (A) Western blot of phospho p38, phospho p44/42 and IκB: Cells were treated with EGF, α-RAGE and HMGB1 and tested at different time points. Results were compared to an untreated control. Tubulin served as a loading control **(B)** Quantification of Western blots. Results were given as fold-change relative to the negative control (dashed line; set to 1). Band intensities were normalized to Tubulin.

As shown in Figure 8, treatment with α-RAGE slightly induced p38 phosphorylation in a time- and dose-dependent manner. The strongest effect was observed when the antibody was added at a concentration of 10 ng/ml for 60 minutes, resulting in a 3.7-fold increased signal compared to the untreated control. Also, when cells were treated with 100 ng/ml HMGB1 increased signals became visible. This effect could not be observed when cells were treated with a higher concentration of HMGB1 (200 ng/ml).

In terms of the ERK 1/2 pathway, stimulation with EGF for 10 and 30 minutes resulted in increased phosphorylation of p44/42, whereas this effect was no longer detectable after 60 minutes. Treatment with α-RAGE at a concentration of 1 ng led to a 2-fold increase in p44/42 phosphorylation expression level. The use of 10 ng/ml α-RAGE resulted in an almost 10-fold increase in p44/42 phosphorylation levels at all time points tested. HMGB1 led to similar activation, however, only after 10 minutes. After 30 and 60 minutes, levels were still increased, but only by a factor of 3 to 4. Adding a higher concentration (200 ng/ml) of HMGB1 resulted in a 4-fold increase after 10 and 30 minutes, and this effect was reduced to a 2-fold increase after 60 minutes.

To test whether treatment with the different substances activates the NF-κB pathway, degradation of IκB was tested by immunoblotting. Reduction of IκB was observed after the use of α-RAGE 1 ng/ml for 10 minutes, leading to a 60 % decrease, whereas this effect was no longer detectable after 30 and 60 minutes. Interestingly, using a higher dosage of α-RAGE (10 ng/ml) resulted in a 1.7 to 2.6 increase of the phosphorylation level of IκB. Stimulation with HMGB1, at the concentration of 100 ng, for 10 minutes showed similar effects. However, after 30 and 60 minutes, this effect could not be observed.

To summarize, α-RAGE and the RAGE ligand HMGB1 led to a strong activation of the ERK 1/2 signaling pathways in Caco-2 cells. Due to time limitations, the effect of AGE-BSA and treatment from the basolateral side could not be tested in this thesis.

3.5. Changes in gene expression after treatment with RAGE ligands

To determine whether treatment of Caco-2 monolayers leads to changes in gene expression, cells were treated with the different RAGE ligands, total RNA was isolated and changes in gene expression were examined by RT-qPCR, following the steps explained in 2.2.8.

3.5.1. Effects on the expression of tight and adherens junction proteins

First, the expression of the selected tight junction proteins, namely Junctional Adhesion Molecule A (JAM-A), Claudin-1 and Claudin-5, as well as adherens junction protein E-cadherin (E-CAD) was analyzed (Figure 9).

The obtained results indicate that apical addition of S100A12, HMGB1 and AGE modified BSA (AGE-BSA) led to a 2 to 6-fold increased expression of all tested tight and adherens junction proteins after one hour. After four hours, this effect was no longer observed, with the exception of E-CAD, which also showed a 2-fold increase in expression after treatment with S100A12 for four hours.

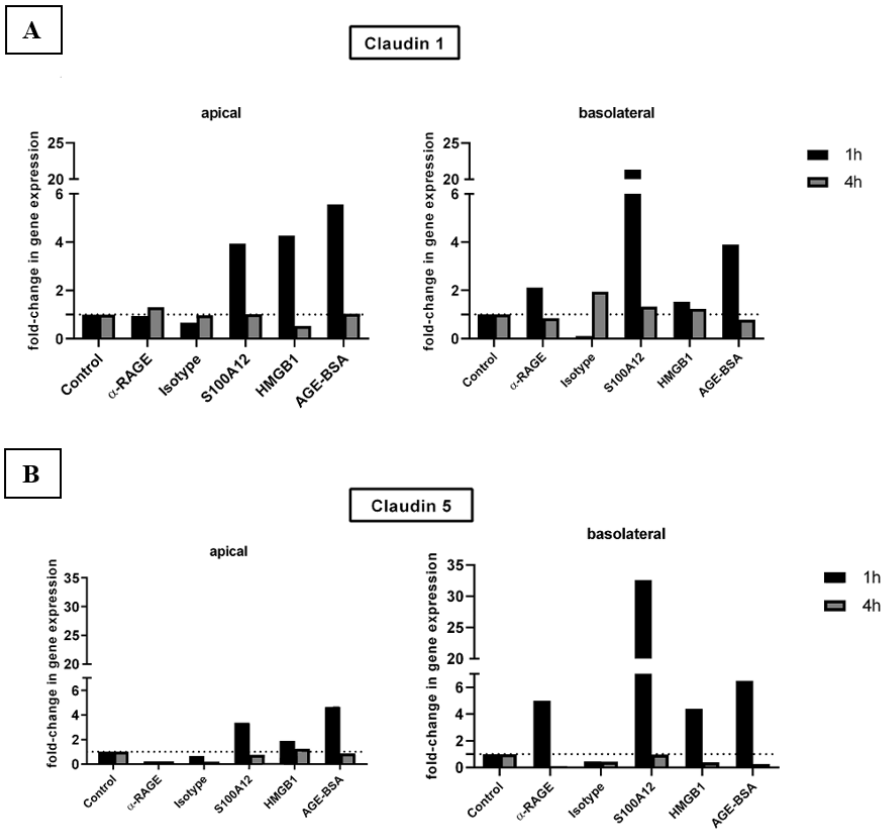

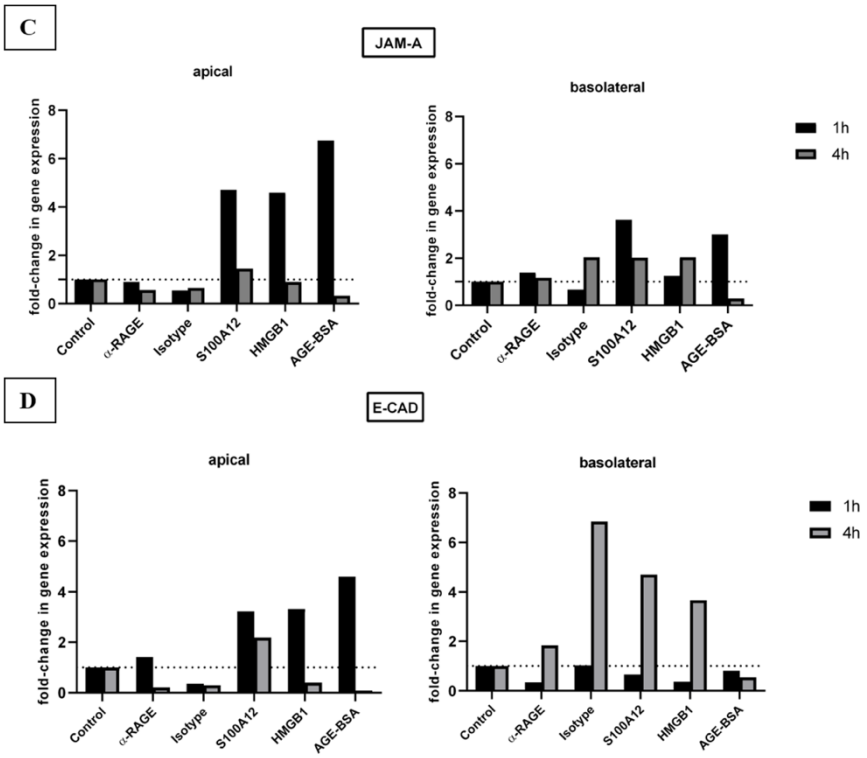

Figure 9. Expression of tight and adherens junctions in Caco-2 cells: Cells were treated with α-RAGE, the isotype control, S100A12, HMGB1 and AGE-modified BSA for one and four hours. Ligands were added either basolaterally or apically. Results were analyzed with RT-qPCR and given as fold-change compared to the negative control (dashed line; set to 1).

Treatment with S100A12 and AGE-BSA from the basolateral side also resulted in an increase in gene expression of Claudin 1, Claudin 5 and JAM-A after one hour, with S100A12 causing a 22 and 32-fold increase in Claudin 1- and Claudin 5-expression, respectively. Interestingly, no such effect was observed for E-CAD after one hour. E-CAD exhibited an upregulation of gene expression after treatment with the isotype control, S100A12 and HMGB1 after four hours, causing a 3 to 7-fold increase compared to the negative control.

After addition of α-RAGE, no noticeable changes in gene expression were observed except for Claudin 1 and Claudin 5 where basolateral treatment for one hour led to a 2 to 5-fold increase.

To summarize, AGE-BSA and other RAGE ligands can change the expression level of selected tight and adherens junction proteins in IECs. Specifically, the addition of RAGE ligands for one hour from the basolateral compartment increased the expression levels of the molecules.

3.5.2. Effects of treatment on cytokine and chemokine expression

Considering the important role of cytokines and chemokines in the regulation and mediation of the inflammatory response, selected cytokines and chemokines were next analyzed for changes in gene expression (Figure 10).

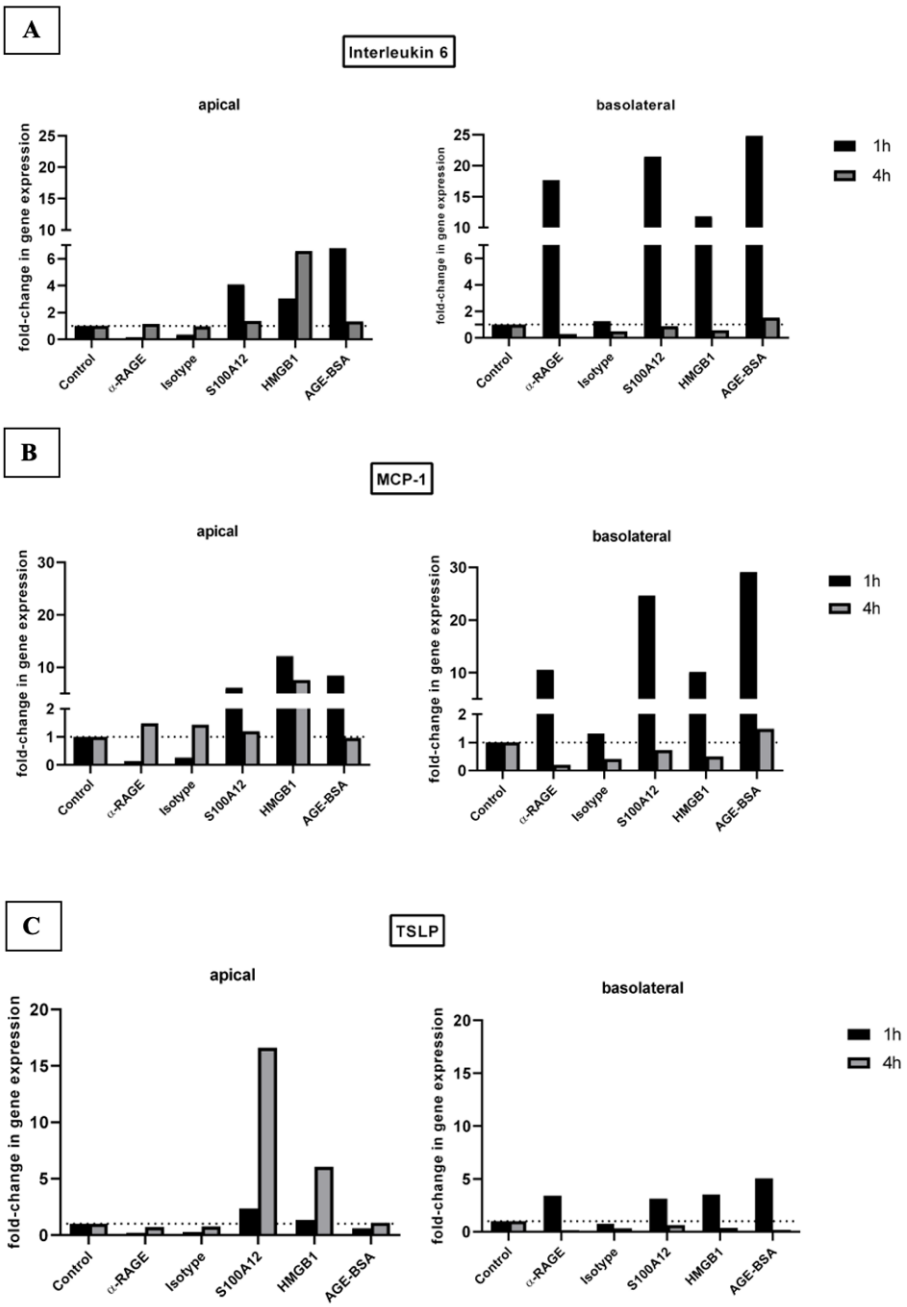

Figure 10. Expression of cytokines and chemokines in Caco-2 cells: Cells were treated with α-RAGE, the isotype control, S100A12, HMGB1 and AGE modified BSA for one and four hours. Ligands were added either basolaterally or apically. Results were analyzed with RT-qPCR and given as fold-change compared to the negative control (dashed line; set to 1)

We examined whether treatment with RAGE-ligands alters the expression of IL-6, MCP-1 (Monocyte Chemoattractant Protein-1) and TSLP (Thymic Stromal Lymphopoietin).

Results of treatment from the apical side showed a change in gene expression of IL-6 when treated with S100A12, HMGB1 and AGE-BSA for one hour. IL-6 gene expression thereby exhibited a 4 to 8-fold increase after addition of S100A12 and AGE-BSA for one hour. Treatment with HMGB1 even led to an increase after both one and four hours, albeit treatment for one hour had a less pronounced effect with only a 2-fold increase in gene-expression.

MCP-1 exhibited results similar to IL-6, with the expection that addition of HMGB1 had a more distinct effect after four-hour treatment, causing a 11-fold increase in gene expression.

Interestingly, TSLP exhibited an upregulation in gene expression after treatment with S100A12 and HMGB1 for four hours, with S100A12 leading to a noticeable 16-fold increase in gene expression.

Regarding the basolateral addition, IL-6 and MCP-1 exhibited an upregulation in gene expression after addition of α-RAGE, S100A12, HMGB1 and AGE-BSA for one hour with a 10 to 30-fold increase. Similar results were observed in TSLP, albeit with a less pronounced effect, resulting only in a 4 to 8-fold increase. After addition for four hours, no such results were observed. The isotope control exhibited no obvious changes in gene expression.

In summary, AGE-BSA and other RAGE ligands altered the gene expression of selected chemokines and cytokines. Specifically, the addition of RAGE ligands for one hour from the basolateral compartment increased the expression levels of the molecules.

3.5.3. Effects on DNA-binding proteins

Since ZBTB20 (Zinc Finger And BTB Domain Containing 20) may be involved in hematopoesis, oncogenesis and immune responses (Zhang et al., 2001) and HMGB1 plays a role in several processes, including inflammation (Yang & Tracey, 2010) we were interested whether treatment with RAGE ligands alters their gene expression (Figure 11).

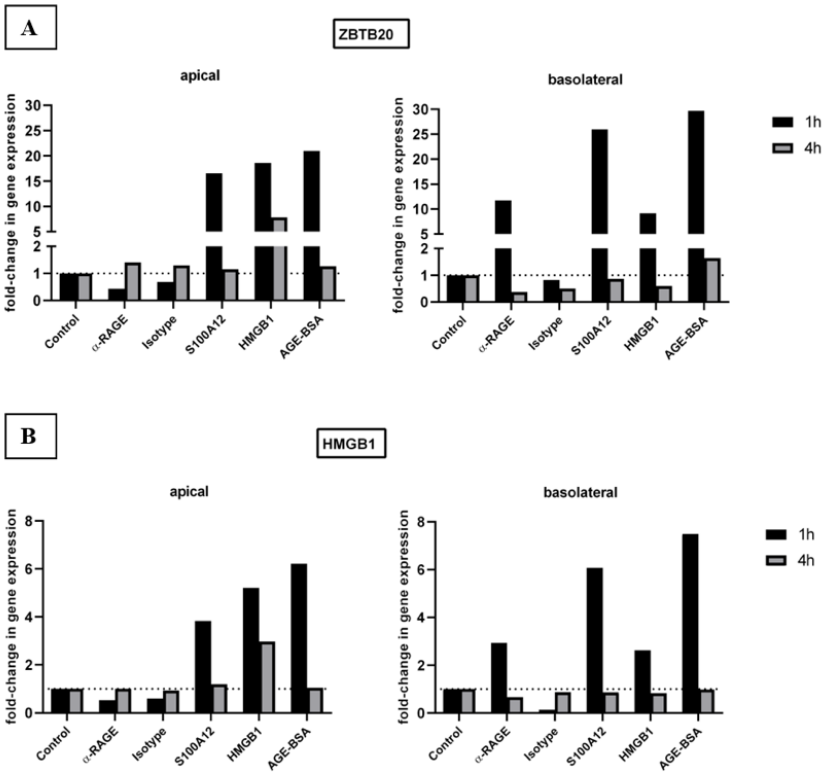

Figure 11. Expression of DNA-binding proteins in Caco-2 cells: Cells were treated with α-RAGE, the isotype control, S100A12, HMGB1 and AGE modified BSA for one and four hours. Ligands were added either basolaterally or apically. Results were

The obtained results of apical addition for ZBTB20 and HMGB1 indicated an increase of gene expression after treatment with S100A12, HMGB1 and BSA-AGE for one hour. Notably, ZBTB20 showed a stronger upregulation compared to HMGB1, with a 15 to 20-fold increase. However, treatment for four hours and addition of α-RAGE for both, one and four hours, showed no remarkable changes.

Treatment with α-RAGE, S100A12, HMGB1 and BSA-AGE from the basolateral side resulted in a 10 to 35-fold increase in gene expression. As expected, addition of the isotope control did not lead to changes in the expression of ZBTB20 and HMGB1.

4. DISCUSSION

AGEs have been recognized for their potential impact on human health, yet there is still a lack of comprehensive studies elucidating how AGEs affect epithelial cells. Therefore, this study investigated the various effects of AGEs in Caco-2 cells, which are an *in vitro* model for human IECs. This study explored the involvement of RAGE in this context by not only analyzing the effects of AGEs but also the effects of other well-described RAGE ligands.

It is described in the literature (Bongarzone et al., 2017; Chiappalupi et al., 2021), that RAGE expression is high in the lung compared to other adult tissues under physiological conditions. In accordance with these data, our results (Figure 4) showed high RAGE-expression levels in lung tissue and lung-derived HBE cells, while relatively low expression was observed in intestinal cell lines, using RT-qPCR. It is worth noting that there were differences in RAGE expression levels among the investigated intestinal cell lines, Caco-2 cells exhibited a higher RAGE expression compared to FHs 74 Int cells. Consequently, and also because Caco-2 cells have the capacity to fully differentiate, further experiments were performed employing the Caco-2 cell model.

To investigate the localization of RAGE within Caco-2 cells, immunofluorescence microscopy was employed. Contrary to the claims in the review (Jansen et al., 2023) suggesting RAGE expression on the lateral side of intestinal cell lines, our results showed apical localization of RAGE in Caco-2 cells. These results suggest that treatment of the apical surface with AGEs may exhibit more pronounced effects compared to basolateral treatment. Interestingly, the results of the experiments did not show more distinct effects after AGEs-treatment on the apical side compared to basolateral treatment, which is discussed later.

It is well-described that Caco-2 cells start to differentiate upon reaching confluence, building a tight cell monolayer due to the formation of tight junctions (Felix et al., 2021; Srinivasan et al., 2015). TEER-measurements are commonly used to monitor the integrity of the cell layer, with TEER values typically increasing in Caco-2 cells over 21 days, reaching the highest value on day 21. Consistent with these studies, our TEER results showed a similar trend, with TEER values reaching a realtively stable value after 20 to 22 days, indicating the formation of a fully functional barrier. Furthermore, we observed an initial increase followed by a slight decrease in TEER values within the first week, followed by a subsequent increase, which aligns with the findings in (Felix et al., 2021). Notably, the high starting value of 600 Ohm*cm^2 at day 5 in our

experiment may be due to a problem during the cell counting process, leading to unintentional over-seeding of cells and thereby a higher TEER-value in the beginning. Therefore, the experiment must be repeated.

Since it has been suggested that several signaling pathways, including ERK 1/2, p38, and NF-κB, are activated after RAGE-ligand interaction (Yeh et al., 2001; Zhu et al., 2012; Zill et al., 2001), we examined the effects of α-RAGE (1 ng/10 ng), EGF and HMGB1 (100 ng/200 ng) on these pathways. Our findings revealed noticeable activation of the ERK 1/2 pathway after stimulation with α-RAGE at a concentration of 10 ng (10, 30, 60 minutes) and HMGB1 100 ng (10 minutes).

However, no noticeable phosphorylation of p38 was observed compared to the untreated control. Thus, this is in contrast to what is mentioned in the literature. This could be due to several factors, for example the used cell type, the culture conditions, the stimulation duration, and the concentration of ligands or antibodies. However, to validate these results and allow for statistical analysis, it is important to repeat the experiment and consider changes in the experimental setting and the use of alternative *in vitro* models.

Furthermore, performed experiments did not support the hypothesis that the NF-κB-pathway may be activated after RAGE-stimulation (Peng et al., 2016; Yeh et al., 2001), as degradation of IκB could not be observed. Interestingly, the results even showed an increase in IκB expression after treatment with α-RAGE 1 ng (10, 30, 60 minutes) and HMGB1 200 ng (10 minutes). However, this could also be due to used experimental settings

To examine RAGE-ligand-dependent changes in gene expression, RT-qPCR was performed. Considering previous reports suggesting that activation of the AGE-RAGE axis can disrupt the intestinal barrier (Rapin & Wiernsperger, 2010; Snelson et al., 2022), we focused on the expression of tight and adherens junctions. Obtained results indicated that apical and basolateral addition of RAGE ligands S100A12, HMGB1 and AGE-BSA for one hour led to an upregulation in gene expression for Claudin 1, Claudin 5 and JAM-A. Basolateral addition even showed an increase after treatment with α-RAGE for one hour regarding Claudin 1 and Claudin 5. Interestlingy, E-CAD showed similar effects, although in terms of basolateral addition, these effects were observed after four-hour instead of one-hour treatment. These findings could support the theory that RAGE-activation leads to the disruption of the intestinal barrier; as a consequence, the cells would probably promote the observed upregulation of gene expression

for tight and adherens junction proteins.This increase would then be able to compensate for the RAGE-induced disruption of intestinal barrier function. Our results showed an increase in TEER after apical and basolateral four-hour treatment with AGEs, which might correlate with the findings from RT-qPCR analyses. The upregulation of gene expression after one-hour treatment leads to the formation of more junctional proteins, resulting in increased TEER values after four hours.

In accordance with the literature (Dong et al., 2022; Sparvero et al., 2009; Yue et al., 2022) suggesting that RAGE-activation, including AGEs-dependent activation, leads to the upregulation of pro-inflammatory factors, we observed an increase in IL-6 and MCP-1 expression after apical and basolateral treatment with S100A12, HMGB1 and AGE-BSA for one hour. Basolateral treatment for one hour even exhibited an increase with α-RAGE.

The pivotal involvement of AGEs and RAGE in activating inflammatory signaling pathways has been well-documented (Cepas et al., 2020; Yan et al., 2008). This association might be linked to the upregulation of ZBTB20 and HMGB1, as these proteins play a role in immune and inflammatory responses. In this study, we in fact observed an upregulation of ZBTB20 and HMGB1 after apical addition of S100A12, HMGB1 and AGE-BSA for one hour. Additionally, basolateral treatment with α-RAGE for one hour also induced an increase in gene expression for ZBTB20 and HMGB1.

Nevertheless, it should be mentioned that Caco-2 cells do not fully represent all characteristics of the IE. Therefore, these limitations need to be taken into account. To address these limitations, co-culture models utilizing Caco-2-cells should be considered. For instance, a co-culture model combining differentiated Caco-2 cells with HT29-MTX cells, which represent mucus-producing cells, has been employed to study the enhanced uptake and transport of nano- and microplastics. Furthermore, co-culture models consisting of Caco-2-cells, dendritic cells, and macrophages have been developed to explore complex interactions within the IE (Paul et al., 2023). Another alternative *in vitro* model proposed for studying the IE is intestinal organoids. These organoids have shown the ability to mimic the 3D architecture, functional characteristics, cell type composition and interaction of the intestinal epithelium (Günther et al., 2022; Taelman et al., 2022).

Also, as the presented data are from a single experiment, at least two more replicates are needed to verify that the analyses are reproducible and also to perform statistical analyses. It is suggested to include other incubation times and investigations with other stimulating factors to gain deeper insights into the effects of AGEs on the intestinal epithelium. Furthermore, this thesis primarly focused on Caco-2 cells. Lung epithelial cell lines may also be of interest to better understand the cellular and molecular mechanisms of RAGE activation, as they exhibit high levels of RAGE expression (Chen et al., 2020).

In conclusion, this thesis focused on investigating the impact of AGEs on Caco-2 cells and the potential interactions with RAGE. RAGE was shown to be more expressed on the apical side of fully differentiated Caco-2 cells and stimulation with RAGE-ligands selectively activated the ERK 1/2 signaling pathway. Increases in gene expression levels were observed for junctional proteins (Claudin 1, Claudin 5, JAM-A, E-CAD), inflammatory and immune factors (IL-6, MCP-1, TSLP, ZBTB20, HMGB1) particularly after one-hour treatment with AGEs. The integrity of the cell monolayer, as measured by TEER, increased after apical and basolateral treatment with AGEs for four hours.

LITERATURE

Bierhaus, A., Humpert, P. M., Morcos, M., Wendt, T., Chavakis, T., Arnold, B., Stern, D. M., & Nawroth, P. P. (2005). Understanding RAGE, the receptor for advanced glycation end products. In *Journal of Molecular Medicine* (Vol. 83, Issue 11, pp. 876–886). https://doi.org/10.1007/s00109-005-0688-7

Bongarzone, S., Savickas, V., Luzi, F., & Gee, A. D. (2017a). Targeting the Receptor for Advanced Glycation Endproducts (RAGE): A Medicinal Chemistry Perspective. In *Journal of Medicinal Chemistry* (Vol. 60, Issue 17, pp. 7213–7232). American Chemical Society. https://doi.org/10.1021/acs.jmedchem.7b00058

Bonis, V., Rossell, C., & Gehart, H. (2021). The Intestinal Epithelium – Fluid Fate and Rigid Structure From Crypt Bottom to Villus Tip. In *Frontiers in Cell and Developmental Biology* (Vol. 9). Frontiers Media S.A. https://doi.org/10.3389/fcell.2021.661931

Boyapati, R. K., Rossi, A. G., Satsangi, J., & Ho, G.-T. (2016). Gut mucosal DAMPs in IBD: from mechanisms to therapeutic implications. *Mucosal Immunology*, *9*(3), 567–582. https://doi.org/10.1038/mi.2016.14

Cao, X., Surma, M. A., & Simons, K. (2012). Polarized sorting and trafficking in epithelial cells. *Cell Research*, *22*(5), 793–805. https://doi.org/10.1038/cr.2012.64

Celebi Sözener, Z., Cevhertas, L., Nadeau, K., Akdis, M., & Akdis, C. A. (2020). Environmental factors in epithelial barrier dysfunction. *Journal of Allergy and Clinical Immunology*, *145*(6), 1517–1528. https://doi.org/10.1016/j.jaci.2020.04.024

Cepas, V., Collino, M., Mayo, J. C., & Sainz, R. M. (2020). Redox Signaling and Advanced Glycation Endproducts (AGEs) in Diet-Related Diseases. *Antioxidants*, *9*(2), 142. https://doi.org/10.3390/antiox9020142

Chellappa, R. C., Palanisamy, R., & Swaminathan, K. (2021). RAGE Isoforms, its Ligands and their Role in Pathophysiology of Alzheimer's Disease. *Current Alzheimer Research*, *17*(14), 1262–1279. https://doi.org/10.2174/1567205018666210218164246

Chen, M.-C., Chen, K.-C., Chang, G.-C., Lin, H., Wu, C.-C., Kao, W.-H., Teng, C.-L. J., Hsu, S.-L., & Yang, T.-Y. (2020). RAGE acts as an oncogenic role and promotes the metastasis of human lung cancer. *Cell Death & Disease*, *11*(4), 265. https://doi.org/10.1038/s41419-020-2432-1

Chiappalupi, S., Salvadori, L., Donato, R., Riuzzi, F., & Sorci, G. (2021a). Hyperactivated RAGE in Comorbidities as a Risk Factor for Severe COVID-19—The Role of RAGE-RAS Crosstalk. *Biomolecules*, *11*(6), 876. https://doi.org/10.3390/biom11060876

Creff, J., Malaquin, L., & Besson, A. (2021). In vitro models of intestinal epithelium: Toward bioengineered systems. In *Journal of Tissue Engineering* (Vol. 12). SAGE Publications Ltd. https://doi.org/10.1177/2041731420985202

Degani, G., Altomare, A. A., Colzani, M., Martino, C., Mazzolari, A., Fritz, G., Vistoli, G., Popolo, L., & Aldini, G. (2017). A capture method based on the VC1 domain reveals new binding properties of the human receptor for advanced glycation end products (RAGE). *Redox Biology*, *11*, 275–285. https://doi.org/10.1016/j.redox.2016.12.017

Dong, H., Zhang, Y., Huang, Y., & Deng, H. (2022a). Pathophysiology of RAGE in inflammatory diseases. In *Frontiers in Immunology* (Vol. 13). Frontiers Media S.A. https://doi.org/10.3389/fimmu.2022.931473

Felix, K., Tobias, S., Jan, H., Nicolas, S., & Michael, M. (2021). Measurements of transepithelial electrical resistance (TEER) are affected by junctional length in immature epithelial monolayers. *Histochemistry and Cell Biology*. https://doi.org/10.1007/s00418-021-02026-4

Gill, V., Kumar, V., Singh, K., Kumar, A., & Kim, J. J. (2019). Advanced glycation end products (AGEs) may be a striking link between modern diet and health. In *Biomolecules* (Vol. 9, Issue 12). MDPI AG. https://doi.org/10.3390/biom9120888

Günther, C., Winner, B., Neurath, M. F., & Stappenbeck, T. S. (2022). Organoids in gastrointestinal diseases: from experimental models to clinical translation. *Gut*, *71*(9), 1892–1908. https://doi.org/10.1136/gutjnl-2021-326560

Hudson, B. I., & Lippman, M. E. (2018). Targeting RAGE Signaling in Inflammatory Disease. *Annual Review of Medicine*, *69*(1), 349–364. https://doi.org/10.1146/annurev-med-041316-085215

Indyk, D., Bronowicka-Szydełko, A., Gamian, A., & Kuzan, A. (2021). Advanced glycation end products and their receptors in serum of patients with type 2 diabetes. *Scientific Reports*, *11*(1), 13264. https://doi.org/10.1038/s41598-021-92630-0

Jansen, F. A. C., Fogliano, V., Rubert, J., & Hoppenbrouwers, T. (2023). Dietary Advanced Glycation End products interacting with the intestinal epithelium: What do we really know? *Molecular Metabolism*, *73*, 101734. https://doi.org/10.1016/j.molmet.2023.101734

Kierdorf, K., & Fritz, G. (2013). RAGE regulation and signaling in inflammation and beyond. *Journal of Leukocyte Biology*, *94*(1), 55–68. https://doi.org/10.1189/jlb.1012519

Kim, H. J., Jeong, M. S., & Jang, S. B. (2021). Molecular characteristics of rage and advances in small-molecule inhibitors. In *International Journal of Molecular Sciences* (Vol. 22, Issue 13). MDPI. https://doi.org/10.3390/ijms22136904

Kleiveland, C., Lea, T., Mackie, A., Requena, T., Swiatecka, D., & Wichers, H. (n.d.). *Kitty Verhoeckx · Paul Cotter Iván López-Expósito The Impact of Food Bioactives on Health In Vitro and Ex Vivo Models*.

Lopez-Escalera, S., & Wellejus, A. (2022). Evaluation of Caco-2 and human intestinal epithelial cells as in vitro models of colonic and small intestinal integrity. *Biochemistry and Biophysics Reports*, *31*. https://doi.org/10.1016/j.bbrep.2022.101314

Moysa, A., Hammerschmid, D., Szczepanowski, R. H., Sobott, F., & Dadlez, M. (2019). Enhanced oligomerization of full-length RAGE by synergy of the interaction of its domains. *Scientific Reports*, *9*(1), 20332. https://doi.org/10.1038/s41598-019-56993-9

Muthyalaiah, Y. S., Jonnalagadda, B., John, C. M., & Arockiasamy, S. (2021). Impact of Advanced Glycation End products (AGEs) and its receptor (RAGE) on cancer metabolic signaling pathways and its progression. *Glycoconjugate Journal*, *38*(6), 717–734. https://doi.org/10.1007/s10719-021-10031-x

Paul, M. B., Schlief, M., Daher, H., Braeuning, A., Sieg, H., & Böhmert, L. (2023). A human Caco-2-based co-culture model of the inflamed intestinal mucosa for particle toxicity studies. *In Vitro Models*, *2*(1–2), 43–64. https://doi.org/10.1007/s44164-023-00047-y

Peng, Y., Kim, J.-M., Park, H.-S., Yang, A., Islam, C., Lakatta, E. G., & Lin, L. (2016). AGE-RAGE signal generates a specific NF-κB RelA "barcode" that directs collagen I expression. *Scientific Reports*, *6*(1), 18822. https://doi.org/10.1038/srep18822

Perrone, A. , G. A. , B. J. , & M. F. (2020). *Advanced Glycation End Products (AGEs): Biochemistry, Signaling, Analytical Methods, and Epigenetic Effects*.

Peterson, L. W., & Artis, D. (2014). Intestinal epithelial cells: Regulators of barrier function and immune homeostasis. In *Nature Reviews Immunology* (Vol. 14, Issue 3, pp. 141–153). https://doi.org/10.1038/nri3608

Ramasamy, R., Shekhtman, A., & Schmidt, A. M. (2022). The RAGE/DIAPH1 Signaling Axis & Implications for the Pathogenesis of Diabetic Complications. *International Journal of Molecular Sciences*, *23*(9), 4579. https://doi.org/10.3390/ijms23094579

Rapin, J. R., & Wiernsperger, N. (2010). Possible Links between Intestinal Permeablity and Food Processing: A Potential Therapeutic Niche for Glutamine. *Clinics*, *65*(6), 635–643. https://doi.org/10.1590/S1807-59322010000600012

Reed, J. C., Preston-Hurlburt, P., Philbrick, W., Betancur, G., Korah, M., Lucas, C., & Herold, K. C. (2020). The receptor for advanced glycation endproducts (RAGE) modulates T cell signaling. *PLoS ONE*, *15*(9 September). https://doi.org/10.1371/journal.pone.0236921

Rescigno, M. (2011). The intestinal epithelial barrier in the control of homeostasis and immunity. *Trends in Immunology*, *32*(6), 256–264. https://doi.org/10.1016/j.it.2011.04.003

Sakaguchi, M., Kinoshita, R., Putranto, E. W., Ruma, I. M. W., Sumardika, I. W., Youyi, C., Tomonobu, N., Yamamoto, K.-I., & Murata, H. (2017). Signal Diversity of Receptor for Advanced Glycation End Products. *Acta Medica Okayama*, *71*(6), 459–465. https://doi.org/10.18926/AMO/55582

Sambuy, Y., De Angelis, I., Ranaldi, G., Scarino, M. L., Stammati, A., & Zucco, F. (2005). The Caco-2 cell line as a model of the intestinal barrier: in£uence of cell and culture-related factors on Caco-2 cell functional characteristics. In *Cell Biology and Toxicology* (Vol. 21). Springer.

Schoultz, I., & Keita, Å. V. (2020). The Intestinal Barrier and Current Techniques for the Assessment of Gut Permeability. In *Cells* (Vol. 9, Issue 8). NLM (Medline). https://doi.org/10.3390/cells9081909

Singh, S., Siva, B. V., & Ravichandiran, V. (2022). Advanced Glycation End Products: key player of the pathogenesis of atherosclerosis. *Glycoconjugate Journal*, *39*(4), 547–563. https://doi.org/10.1007/s10719-022-10063-x

Snelson, M., Lucut, E., & Coughlan, M. T. (2022b). The Role of AGE-RAGE Signalling as a Modulator of Gut Permeability in Diabetes. In *International Journal of Molecular Sciences* (Vol. 23, Issue 3). MDPI. https://doi.org/10.3390/ijms23031766

Sparvero, L. J., Asafu-Adjei, D., Kang, R., Tang, D., Amin, N., Im, J., Rutledge, R., Lin, B., Amoscato, A. A., Zeh, H. J., & Lotze, M. T. (2009). RAGE (Receptor for Advanced Glycation Endproducts), RAGE Ligands, and their role in Cancer and Inflammation. *Journal of Translational Medicine*, *7*(1), 17. https://doi.org/10.1186/1479-5876-7-17

Srinivasan, B., Kolli, A. R., Esch, M. B., Abaci, H. E., Shuler, M. L., & Hickman, J. J. (2015). TEER Measurement Techniques for In Vitro Barrier Model Systems. *SLAS Technology*, *20*(2), 107–126. https://doi.org/10.1177/2211068214561025

Taelman, J., Diaz, M., & Guiu, J. (2022). Human Intestinal Organoids: Promise and Challenge. *Frontiers in Cell and Developmental Biology*, *10*. https://doi.org/10.3389/fcell.2022.854740

Taguchi, K., & Fukami, K. (2023). RAGE signaling regulates the progression of diabetic complications. *Frontiers in Pharmacology*, *14*. https://doi.org/10.3389/fphar.2023.1128872

Tsang, M., Gantchev, J., Ghazawi, F. M., & Litvinov, I. V. (2017). Protocol for adhesion and immunostaining of lymphocytes and other non-adherent cells in culture. *BioTechniques*, *63*(5), 230–233. https://doi.org/10.2144/000114610

Twarda-clapa, A., Olczak, A., Białkowska, A. M., & Koziołkiewicz, M. (2022a). Advanced Glycation End-Products (AGEs): Formation, Chemistry, Classification, Receptors, and Diseases Related to AGEs. In *Cells* (Vol. 11, Issue 8). MDPI. https://doi.org/10.3390/cells11081312

Yan, S. F., Ramasamy, R., & Schmidt, A. M. (2008). Mechanisms of Disease: advanced glycation end-products and their receptor in inflammation and diabetes complications. *Nature Clinical Practice Endocrinology & Metabolism*, *4*(5), 285–293. https://doi.org/10.1038/ncpendmet0786

Yang, H., & Tracey, K. J. (2010). Targeting HMGB1 in inflammation. *Biochimica et Biophysica Acta (BBA) - Gene Regulatory Mechanisms*, *1799*(1–2), 149–156. https://doi.org/10.1016/j.bbagrm.2009.11.019

Yeh, C.-H., Sturgis, L., Haidacher, J., Zhang, X.-N., Sherwood, S. J., Bjercke, R. J., Juhasz, O., Crow, M. T., Tilton, R. G., & Denner, L. (2001). Requirement for p38 and p44/p42 Mitogen-Activated Protein Kinases in RAGE-Mediated Nuclear Factor-κB Transcriptional Activation and Cytokine Secretion. *Diabetes*, *50*(6), 1495–1504. https://doi.org/10.2337/diabetes.50.6.1495

Yubero-Serrano, E. M., & Pérez-Martínez, P. (2020). Advanced Glycation End Products and Their Involvement in Cardiovascular Disease. *Angiology*, *71*(8), 698–700. https://doi.org/10.1177/0003319720916301

Yue, Q., Song, Y., Liu, Z., Zhang, L., Yang, L., & Li, J. (2022). Receptor for Advanced Glycation End Products (RAGE): A Pivotal Hub in Immune Diseases. *Molecules*, *27*(15), 4922. https://doi.org/10.3390/molecules27154922

Zhang, W., Mi, J., Li, N., Sui, L., Wan, T., Zhang, J., Chen, T., & Cao, X. (2001). Identification and Characterization of DPZF, a Novel Human BTB/POZ Zinc Finger Protein Sharing

Homology to BCL-6. *Biochemical and Biophysical Research Communications*, *282*(4), 1067–1073. https://doi.org/10.1006/bbrc.2001.4689

Zhu, P., Ren, M., Yang, C., Hu, Y.-X., Ran, J.-M., & Yan, L. (2012). Involvement of RAGE, MAPK and NF-κB pathways in AGEs-induced MMP-9 activation in HaCaT keratinocytes. *Experimental Dermatology*, *21*(2), 123–129. https://doi.org/10.1111/j.1600-0625.2011.01408.x

Zill, H., Günther, R., Erbersdobler, H. F., Fölsch, U. R., & Faist, V. (2001). RAGE Expression and AGE-Induced MAP Kinase Activation in Caco-2 Cells. *Biochemical and Biophysical Research Communications*, *288*(5), 1108–1111. https://doi.org/10.1006/bbrc.2001.5901

FIGURES AND TABLES